Recovery of respiratory function in *mdx* mice co-treated with neutralizing interleukin-6 receptor antibodies and Urocortin-2

David P. Burns[1], Leonie Canavan[2], Jane Rowland[2], Robin O'Flaherty[1], Molly Brannock[2], Sarah E. Drummond[1], Dervla O'Malley[1], Deirdre Edge[2] and Ken D. O'Halloran[1,*]

[1]Department of Physiology, School of Medicine, College of Medicine & Health, University College Cork, Cork, Ireland;

[2]Department of Physiology, School of Medicine, Trinity Biomedical Sciences Institute, Trinity College Dublin, the University of Dublin, Dublin, Ireland

***Corresponding author**

Professor Ken D. O'Halloran, PhD | Department of Physiology, Western Gateway Building, Western Road, Cork, Ireland | Tel: +353-21-4205433 | k.ohalloran@ucc.ie

Short title: Combined drug therapy improves breathing in *mdx* mice.

Subject area: Muscle physiology

Total number of references: 62

Abbreviations: ANOVA, analysis of variance; BB_n, breath-to-breath; BB_{n+1}, breath-to-breath interval; CRFR, corticotrophin releasing factor receptor; CSA, cross-sectional area; CT, contraction time; DMD, Duchenne muscular dystrophy; F_iO_2, fractional inspired oxygen concentration; f_R, respiratory frequency; IL, interleukin; IL-6R, IL-6 receptor; L_o, optimum length; MyHC, myosin heavy chain; OCT, optimum cutting temperature; Pmax, maximum mechanical power; SD1, short-

This is an Accepted Article that has been peer-reviewed and approved for publication in the The Journal of Physiology, but has yet to undergo copy-editing and proof correction. Please cite this article as an 'Accepted Article'; doi: 10.1113/JP276954.

term variability; SD2, long-term variability; Smax, maximum total shortening; T_e, expiratory duration; T_i, inspiratory duration; TNF-α, tumor necrosis factor alpha; Ucn2, Urocortin-2; Vmax, maximum shortening velocity; $\dot{V}_E$, minute ventilation; $\dot{V}_E/\dot{V}CO_2$, ventilatory equivalent for carbon dioxide; $\dot{V}_E/\dot{V}O_2$, ventilatory equivalent for oxygen; $\dot{V}CO_2$, carbon dioxide production; $\dot{V}O_2$, oxygen consumption; V_T, tidal volume; Wmax, maximum mechanical work; WT, wild-type; xIL-6R, anti-IL-6R; ½ RT, half relaxation time.

Key points summary

- Impaired ventilatory capacity and diaphragm muscle weakness are prominent features of Duchenne muscular dystrophy (DMD), with strong evidence of attendant systemic and muscle inflammation.
- We performed a two-week intervention in young wild-type and *mdx* mice, consisting of either injection of saline or co-administration of a neutralizing interleukin-6 receptor antibody (xIL-6R) and Urocortin-2 (Ucn2), a corticotrophin releasing factor receptor 2 agonist. We examined breathing and diaphragm muscle form and function.
- Breathing and diaphragm muscle functional deficits are improved following xIL-6R and Ucn2 co-treatment in *mdx* mice. The functional improvements were associated with a preservation of *mdx* diaphragm muscle myosin heavy chain IIx fibre complement.
- The concentration of the pro-inflammatory cytokine interleukin-1β was reduced and the concentration of the anti-inflammatory cytokine interleukin-10 was increased in *mdx* diaphragm following drug co-treatment.
- Our novel findings may have implications for the development of pharmacotherapies for the dystrophinopathies with relevance for respiratory muscle performance and breathing.

Abstract

The *mdx* mouse model of Duchenne muscular dystrophy shows evidence of hypoventilation and pronounced diaphragm dysfunction. Six-week-old male *mdx* (n=32) and wild-type (WT; n=32) mice received either saline (0.9% w/v) or a co-administration of neutralizing interleukin-6 receptor

antibodies (xIL-6R; 0.2 mg/kg) and corticotrophin-releasing factor receptor 2 agonist (Urocortin-2; 30 μg/kg), subcutaneously over 2 weeks. Breathing and diaphragm muscle contractile function (*ex vivo)* were examined. Diaphragm structure was assessed using histology and immunofluorescence. Muscle cytokine concentration was determined using a multiplex assay. Minute ventilation and diaphragm muscle peak force at 100 Hz were significantly depressed in *mdx* compared with WT. Drug treatment completely restored ventilation in *mdx* mice during normoxia and significantly increased *mdx* diaphragm force- and power-generating capacity. The number of centrally-nucleated muscle fibres and the areal density of infiltrates and collagen content were significantly increased in *mdx* diaphragm; all indices were unaffected by drug co-treatment. The abundance of myosin heavy chain (MyHC) type IIx fibres was significantly decreased in *mdx* diaphragm; drug co-treatment preserved MyHC type IIx complement in *mdx* muscle. Drug co-treatment increased the cross-sectional area of MyHC type I and IIx fibres in *mdx* diaphragm. The cytokines IL-1β, IL-6, KC/GRO and TNF-α were significantly increased in *mdx* diaphragm compared with WT. Drug co-treatment significantly decreased IL-1β and increased IL-10 in *mdx* diaphragm. Drug co-treatment had no significant effect on WT diaphragm muscle structure, cytokine concentrations or function. Recovery of breathing and diaphragm force in *mdx* mice was impressive in our studies, with implication for human dystrophinopathies.

Keywords

DMD; *mdx*; interleukin-6; Urocortin-2; corticotrophin releasing factor; diaphragm muscle; breathing.

1. Introduction

Duchenne muscular dystrophy (DMD) is a fatal neuromuscular disease wherein patients lack the structural protein dystrophin. In the absence of dystrophin, extensive skeletal muscle weakness, damage and fibre remodelling occurs (Blake *et al.*, 2002). Weakness extends to the striated muscles of breathing, with patients displaying diaphragm muscle dysfunction (De Bruin *et al.*, 1997; Khirani *et al.*, 2014) with consequential respiratory disturbance (Smith *et al.*, 1989; Khan & Heckmatt, 1994) and disrupted blood gas homeostasis (Smith *et al.*, 1988).

Similar to DMD, the *mdx* mouse model of DMD shows evidence of diaphragmatic dysfunction and impaired ventilation (Stedman *et al.*, 1991; Coirault *et al.*, 1999; Mosqueira *et al.*, 2013; Burns *et al.*, 2015; Burns *et al.*, 2017c). Skeletal muscle weakness due to dystrophin deficiency is further driven by pathological changes due to extensive muscle damage, including muscle fibre degeneration and necrosis, fibrosis, inflammation and adipose tissue deposition. Inflammation is a secondary feature of DMD due to muscle damage caused by the absence of dystrophin (Deconinck & Dan, 2007). Inflammatory cells infiltrate damaged muscles mounting an inflammatory response through activation of cytokines and recruitment of additional immune cells to the damaged muscle (De Paepe & De Bleecker, 2013).

The expression of inflammatory cytokines is elevated in muscle biopsies and plasma samples from DMD patients and the *mdx* mouse model of DMD, some of which include tumor necrosis factor (TNFα), interleukin-1 (IL-1) and interleukin-6 (IL-6) (Chahbouni *et al.*, 2010; Messina *et al.*, 2011; Pelosi *et al.*, 2015a). IL-6 is considered a myokine that can be released from damaged muscle in response to muscle injury and is pleiotropic in nature. IL-6 exerts its pro-inflammatory actions via its trans-signalling pathway, mediated by the soluble IL-6 receptor (IL-6R). Recent studies examining blockade of IL-6 signalling in *mdx* mice have shown functional improvements in skeletal and smooth muscle (Pelosi *et al.*, 2015a; Manning *et al.*, 2016, 2017).

Muscle fibre loss occurs in DMD, with necrotic muscle fibres replaced by connective and adipose tissue. Signalling through the corticotrophin releasing factor receptor (CRFR) has been shown to modulate muscle mass. Activation of CRFR2 (expressed in skeletal muscle) in mice has been shown to increase muscle mass and prevent muscle mass and function loss in atrophying muscle (Hinkle *et al.*, 2003a; Hinkle *et al.*, 2003b; Hinkle *et al.*, 2004). Similarly, the CRFR2 agonist Urocortin-2 (Ucn2) has been demonstrated to increase muscle mass and force in *mdx* mice (Reutenauer-Patte *et al.*, 2012; Manning *et al.*, 2017). Moreover, Ucn2 has been shown to exert beneficial effects on cardiac function in healthy subjects and heart failure patients (Stirrat *et al.*, 2016).

A recent study has demonstrated that neutralization of the IL-6R (xIL-6R) and stimulation of CRFR2 (Ucn2) via a combined drug strategy in young *mdx* mice leads to beneficial improvements in

diaphragm muscle functional capacity, with co-treatment proving more effective than either drug administered independently due to additive inotropic effects (Manning *et al.*, 2017). Combined treatment with xIL-6R and Ucn2 restored diaphragm muscle functional deficits in *mdx* mice, evidenced by improved force, work and muscle shortening capacity (Manning *et al.*, 2017). Similarly, a co-treatment of xIL-6R and Ucn2 completely recovered pharyngeal dilator (sternohyoid) muscle force and power loss in *mdx* mice (Burns *et al.*, 2017b). Co-treatment preserved the myosin heavy chain (MyHC) fibre complement and reduced the number of centrally-nucleated fibres in sternohyoid muscle, suggesting a reduction in muscle fibre damage (Burns *et al.*, 2017b). We sought to build considerably on this previous work, extending studies to breathing, diaphragm muscle physiology and structural composition, as well as diaphragm cytokine profiles in young adult (8 weeks of age) wild-type and *mdx* mice following saline or combined xIL-6R and Ucn2 drug treatment.

We hypothesized that drug co-treatment would reduce inflammation and improve the quality of diaphragm muscle, preserving muscle fibre type distribution. We further hypothesized that co-administration of xIL-6R antibodies and Ucn2 would improve diaphragm muscle force-generating capacity and ventilatory capacity in *mdx*.

2. Methods

2.1 Ethical approval

Procedures on live animals were performed under licence in accordance with Irish and European directive 2010/63/EU following ethical approval by University College Cork (AEEC #2013/035). Experiments were carried out in accordance with guidelines laid down by University College Cork Animal Welfare Body, and conform to the principles and regulations described by Grundy (2015).

2.2 Animals

Male and female WT (C57BL/10ScSnJ) and *mdx* (C57BL/10ScSn-Dmd^{mdx}/J) mice were purchased from the Jackson Laboratory (Jackson Laboratory, Bar Harbor, ME, USA) and were bred in our institution's animal housing facility. Animals were housed conventionally in a temperature- and

humidity-controlled facility, operating on a 12 h light:12 h dark cycle with food and water available *ad libitum*. Six-week-old male WT and *mdx* mice received an interventional drug treatment consisting of a co-administration of xIL-6R (IL-6R neutralizing antibody; MR16-1 (Okazaki *et al.*, 2002); 0.2 mg/kg; Chugai Pharmaceuticals, Chuo, Tokyo, Japan) and Ucn2 (CRFR2 agonist; 30 μg/kg; U9507; Sigma Aldrich, Wicklow, Ireland) or saline (vehicle control; 0.9% w/v). MR16-1 stock was stored at -80^{o}C and Ucn2 stock was stored at -20^{o}C. A working solution containing both MR16-1 (26.7μg/ml) and Ucn2 (4μg/ml) was made in sterile saline, distributed in aliquots and stored at -20^{o}C until day of injection. The doses and treatment protocol were chosen based on previous studies by our research group (Manning *et al.*, 2016; Manning *et al.*, 2017). Drug treatment consisted of a total of six consecutive subcutaneous injections to the scruff of the neck, each on alternate days over the course of two weeks beginning at 6 weeks of age. Animals were injected with a 7.5 μl bolus per gram body mass. Male WT and *mdx* mice were assigned at random to saline or drug treatment, establishing the following four groups: WT + saline, WT + treatment, *mdx* + saline and *mdx* + treatment. Animals were anaesthetized with 5% isoflurane by inhalation in air and euthanized by cervical dislocation. A study of sternohyoid muscle form and function from these mice was published previously (Burns *et al.*, 2017b).

2.3 Respiratory measurements

Whole body plethysmography was used to examine ventilation in unrestrained and unanaesthetized mice during quiet rest. Mice from all four groups were studied: WT + saline (n = 14), WT + treatment (n = 10), *mdx* + saline (n = 10) and *mdx* + treatment (n = 12). Mice were introduced into plethysmograph chambers (Model PLY4211; volume=0.6L, Buxco Research Systems, Wilmington, NC, USA) and allowed a 60-90 minute acclimation period until sufficiently settled, with room air passing through each chamber (1 L/min). *Experimental protocol*: Following acclimation, a 20-30 minute baseline recording was performed in normoxia. This was followed by a 20 minute hypoxic challenge (F_iO_2 = 0.1; balance N_2). Following a 60 minute recovery in normoxia, a 20-30 minute normoxic baseline was recorded. Following this period, ventilatory responses to hypercapnic challenge (5% CO_2; balance O_2) were assessed in mice from all four groups. Unfortunately, technical issues encountered in two groups (WT + treatment and *mdx* + treatment) relating to inaccurate pre-calibrated gases necessitated exclusion of the complete data set, limiting comparisons to WT + saline versus *mdx* + saline during hypercapnic ventilation. Respiratory parameters including respiratory

frequency (f_R), tidal volume (V_T), minute ventilation (V_E), inspiratory duration (T_i) and expiratory duration (T_e) were recorded on a breath-by breath basis for analysis offline. *Data analysis*: For the assessment of ventilatory parameters in normoxia, both normoxia bouts were pooled to generate one set of baseline (normoxia) data after confirming that there was no significant difference for ventilatory parameters between the two normoxic periods in order to provide a broader characterization of breathing over longer recording periods consistent with the approach in our recent study (Burns *et al*. 2017c). For the hypoxic gas challenge, data during hypoxia are compared with the preceding baseline period and data are presented on a minute-by-minute basis thereafter. Peak ventilation during hypoxia was determined over a period of one minute during 1-3 minutes of exposure when peak responses were observed. V_T and V_E were normalized for body mass (g). To assess respiratory stability during normoxia, the breath-to-breath (BB_n) and subsequent interval (BB_{n+1}) of 200 consecutive breaths were analysed. Short-term variability (SD1) and long-term variability (SD2) were calculated for all four groups (Peng *et al.*, 2011; Souza *et al.*, 2015).

2.4 Metabolism measurements

O_2 consumption ($\dot{V}O_2$) and CO_2 production ($\dot{V}CO_2$) were measured in mice undergoing the whole-body plethysmography protocol during normoxic baseline periods and during exposure to hypoxia. Airflow through the chamber was maintained at 1 L/min. Fractional concentrations of O_2 and CO_2 were measured in air entering and exiting the plethysmograph (O_2 and CO_2 analyser; ADInstruments, Colorado Springs, CO, USA) as previously described (Burns *et al.*, 2017c). *Data analysis:* Calculation of $\dot{V}O_2$ and $\dot{V}CO_2$ was performed as previously described (Haouzi *et al.*, 2009; Burns *et al.*, 2017c). For the 20 min hypoxic challenge, metabolic-related data are shown after 5 min of exposure to ensure steady-state responses and complete washout of chamber gas and are presented on a minute-by-minute basis thereafter. The plethysmograph chamber volume used in the current study was 0.6L and flow rate was 1L/min. We assume that washout was effective by 5 tau i.e. ~3 minutes. It is essential that metabolism is assessed in steady-state conditions with the chamber fully equilibrated and so for these reasons data are expressed only from the 5th minute in hypoxic challenges. This is consistent with the approach taken in our recent study (Burns *et al*. 2017c) and by others in the field. Data during hypoxia exposure were compared with the preceding baseline (F_iO_2 = 0.21) so as to determine the ventilatory and metabolic response to challenge. $\dot{V}O_2$ and $\dot{V}CO_2$ were normalized for body mass (g).

2.5 Tissue collection

The distance from nose-to-anus and nose-to-tail was examined postmortem as an index of somatic growth. The diaphragm muscle was excised with rib and central tendon intact and placed in a tissue bath at room temperature containing continuously gassed hyperoxic (95% O_2/ 5% CO_2) Krebs solution (in mM: NaCl, 120; KCl, 5; Ca^{2+} gluconate, 2.5; $MgSO_4$, 1.2; NaH_2PO_4, 1.2; $NaHCO_3$, 25; and glucose, 11.5) and *d*-tubocurarine (25μM) prior to functional analysis. The following organs and muscles were weighed (wet weight): spleen, lung, whole heart, right heart ventricle, left heart ventricle, tibialis anterior, extensor digitorum longus and soleus.

2.6 Muscle physiology

2.6.1 Ex vivo *muscle preparation*

One costal portion of the diaphragm was used immediately for functional analysis and the other portion was snap frozen in liquid nitrogen and stored at -80^{o}C for subsequent molecular analysis. Longitudinally arranged bundles were prepared for assessment of contractile function. A single longitudinal strip (2 mm in diameter) for each animal was suspended vertically between two platinum plate electrodes. Rib was attached to a fixed hook at one end and the central tendon was attached to a dual-mode lever transducer system (Aurora Scientific Inc.; Aurora, ON, Canada) by non-elastic string. Muscle preparations were studied in a water-jacketed muscle bath, containing Krebs solution, maintained at 35^{o}C gassed with 95% O_2/ 5% CO_2. Preparations were allowed a 5 min equilibration period.

2.6.2 Isometric protocol

Following equilibration, the optimum length (L_o) was determined by adjusting the position of the force transducer by use of a micro-positioner between intermittent twitch contractions. The L_o was taken as the muscle length associated with maximal isometric twitch force in response to single isometric twitch stimulation (supramaximal stimulation, 1ms duration). Once L_o was determined, the muscle stayed at this length for the duration of the protocol. A single isometric twitch was measured.

Peak isometric twitch force, contraction time (CT; time to peak force) and half relaxation time (½ RT; time for peak force to decay by 50%) were determined. Next, an isometric tetanic contraction was elicited by stimulating muscle strips with supramaximal voltage at 100 Hz for 300 ms duration. Peak isometric tetanic force was determined at 100Hz (O'Halloran, 2006; Burns & O'Halloran, 2016). *Data analysis*: Force was calculated in N/cm^2 of muscle bundle cross-sectional area (CSA). The CSA of each muscle strip was determined by dividing the muscle mass (weight in grams) by the product of muscle L_o (cm) and muscle density (assumed to be 1.06 g/cm^3). Normalizing force to muscle bundle CSA accounted for potential differences between preparations in the size of the bundle, notwithstanding that the preparation of muscle strips for study was standardized. We deemed this approach to be more appropriate than representation of absolute forces, although the outcomes of our study proved similar whether absolute or normalized forces were compared between groups. However, we acknowledge that muscle density is likely to differ between WT and *mdx* due to collagen deposition in dystrophic muscle. The CT and ½ RT were measured as indices of isometric twitch kinetics.

2.6.3 Isotonic protocol

Following the isometric protocol, concentric contractions were elicited in incremental steps with varying load (0%, 5%, 10%, 15%, 20%, 25%, 30%, 35%, 40%, 60%, 80, 100; % of force at 100Hz), with 30 s rest between each contraction. Muscle length returned to L_o following each contraction. Total shortening was determined as the maximum distance shortened during contraction. Shortening velocity was determined as the distance shortened during the initial 30 ms of shortening (Lewis *et al.*, 2015; Lewis *et al.*, 2016). Mechanical work (force x total shortening) and power (force x shortening velocity) were determined at each step of the incremental load step test (Lewis *et al.*, 2015; Williams *et al.*, 2015; Burns & O'Halloran, 2016; O'Leary & O'Halloran, 2016). *Data analysis*: Data were plotted as the measured variable versus % load. Total muscle shortening was normalised to L_o and expressed in L/L_o. Similarly, shortening velocity was normalised to L_o and expressed in L_o/s. Maximum total shortening (Smax) and maximum shortening velocity (Vmax) were measured when both were maximal at 0% load. Mechanical work was measured in J/cm^2. Mechanical power was expressed in W/cm^2. Maximum mechanical work (Wmax) and power (Pmax) were also measured and typically occurred between 30% and 40% load.

2.7 Muscle immunohistochemistry and histology

2.7.1 Tissue preparation

A section of the diaphragm muscle was excised and mounted on a cube of liver, allowing for a transverse orientation of muscle fibres. The tissue was covered in optimum cutting temperature (OCT; VWR International, Dublin, Ireland) embedding medium and frozen in isopentane cooled in liquid nitrogen and stored at -80^{o}C for subsequent structural analysis (n = 4-5 per group). A separate section of the muscle was placed in 4% paraformaldehyde overnight at 4^{o}C before being transferred to 70% ethanol prior to tissue processing (Leica TP1020, Histokinet; Leica Biosystems, Dublin, Ireland) and paraffin embedding (Sakura Tissue-Tek TEC, Histolab Histowax embedding medium), for histological analysis (n = 4-5 per group).

2.7.2 Myosin heavy chain fluorescence immunohistochemistry

Serial transverse sections (10µm) were cryosectioned (Model CM30505; Leica Microsystems, Nussloch, Germany) at –22ºC and mounted on polylysine-coated glass slides (VWR International). Two slides per animal from 2 distinct regions containing a minimum of 4 sections per slide were processed for MyHC immunofluorescence. A hydrophobic pen (ImmEdge^{TM}; Vector Laboratories Ltd., Peterborough, UK) was used to circumscribe each section on the slide, creating a well allowing for the containment of antibodies and to stop cross-reactivity of antibodies between muscle sections. Slides were immersed in phosphate-buffered saline (0.01M PBS; Sigma-Aldrich, Wicklow, Ireland) containing 1% bovine serum albumin (BSA; Sigma-Aldrich) for 15 mins, followed by three 5 min PBS rinses. This was followed by a 30 min wash in PBS containing 5% goat serum (Sigma-Aldrich). Before application of the primary mouse monoclonal antibodies (developed by S. Schiaffino and obtained from the Developmental Studies Hybridoma Bank (DSHB) at the University of Iowa, IA, USA), slides were subject to a further blocking step to enable the use of mouse monoclonal primary antibody staining on mouse tissue. Slides were incubated for 1 hour at room temperature with an unconjugated AffiniPure Fab Fragment Goat Anti-Mouse IgG (1:13; Jackson ImmunoResearch Labs, West Grove, PA, USA) diluted in PBS, followed by three 2 min washes in PBS. A triple-labelled approach was used to tag the 3 principal myosin isoforms using a cocktail of antibodies that targeted MyHC types I (BAD5, 1:100), IIa (sc71 1:100) and IIb (BFF3 1:100) on a single section. On a serial

section a double-labelled approach was employed using a cocktail which consisted of a rabbit anti-laminin antibody (1:500, Sigma-Aldrich) and a pan-MyHC antibody for the indirect determination of pure MyHC IIx fibres, BF35 (1:50), labelling all MyHC isoforms but IIx, enabling visualization of IIx fibres by the absence of staining. The antibodies were diluted in PBS and 1% BSA and were incubated overnight at 4°C in a humidity chamber. Following this, slides were rinsed for three 5 min washes in PBS before application of the relevant secondary antibodies, diluted in PBS and 1% BSA. A cocktail of secondary antibodies was prepared containing AlexaFluor350-conjugated goat anti-mouse IgG2b (1:500, Invitrogen, Biosciences Ltd, Dun Laoghaire, Ireland), Dylight594-conjugated goat anti-mouse IgG1 (1:500; Jackson ImmunoResearch) and AlexaFluor488-conjugated goat anti-mouse IgM (1:250; Invitrogen), targeting MyHC I, IIa and IIb, respectively. For the double-labelled sections a Dylight594-conjugated goat anti-mouse IgG_1 (1:500; Jackson) and FITC-conjugated anti-rabbit secondary antibody (1:250; Sigma-Aldrich) were applied for 1 hour in the dark at room temperature. Slides were rinsed with PBS for three 5 min washes, cover slipped with polyvinyl alcohol (PVA) mounting medium with DABCO® anti-fade (Sigma-Aldrich) before observation with a fluorescent microscope (Olympus BX51). Negative control experiments were run in parallel where the primary antibodies were omitted and the secondary antibodies were applied to ensure that tagging was specific. Slides for MyHC immunohistochemistry were processed in parallel across all 4 groups and confocal image acquisition was performed with standardized exposure settings. *Data analysis*: For MyHC fibre type analysis, muscle sections were viewed at x10 magnification and images captured using an Olympus BX51 microscope and an Olympus DP71 camera. Cell Sens™ (Olympus) was used to digitally capture the images. Analysis was carried out using image J software, where fibre type CSA and fibre type distribution (areal density) for each MyHC fibre type were determined (Burns *et al.*, 2017b). For each animal, multiple sections throughout the muscle were viewed and 3-4 images analysed per fibre type.

2.7.3 Histological analysis

Paraffin embedded diaphragm muscle samples were sectioned using a microtome (Leica RM2135). Serial cross-sections (5 μm thick) were collected throughout the muscle (mid-belly and distal regions) onto polylysine coated glass slides (VWR) and oven-dried (overnight at 37°C) for histological analysis. To examine putative inflammatory cell infiltration, and central nucleation of muscle fibres, tissue sections were stained with Haematoxylin and Eosin (H&E). For collagen staining, a Masson's

trichrome protocol was followed (Sigma-Aldrich). Slides were mounted using DPX mounting medium (Sigma-Aldrich, USA), air-dried and visualized on a bright field microscope (Olympus BX51) at x20 magnification. For H&E staining, slides were processed using muscle sections from all 4 groups using the same reagents. Batches were processed in iterative fashion. Occasionally, it was necessary to re-run the histology with new sections but this always included a selection of slides from different experimental groups. Brightness was adjusted within each imaging session for optimal images. For Masson's Trichrome staining, tissue sections were processed in batches ensuring equivalent incubation times across all 4 groups in parallel using the same reagents. Contrast and brightness was standardized as this was important for colour thresholding during image analysis. This was carefully and rigorously controlled. *Data analysis:* H&E stained sections were visualized at x20 magnification. Six sections were examined across the muscle from the rostral, middle and caudal regions. Two randomly selected areas were captured per muscle section from non-overlapping areas for analysis. Muscle pathology was scored using ImageJ software. The number of myofibres displaying central nucleation was expressed as a percentage of the total number of myofibres per image. Putative inflammatory cell infiltration (the presence of cells in the extracellular matrix) was also scored and expressed as a percentage of the total area of muscle. Three sections, with two images captured per section, from the mid-portion of the muscle, were analysed per animal. Images were analysed using a colour balance threshold (ImageJ software), and the area of collagen was expressed as a percentage of the total area of muscle.

2.7.4 Fluorescently-labelled collagen binding protein

Additional collagen staining of the diaphragm muscle was carried out using a fluorescent collagen marker (CNA35-OG488), developed by (Krahn *et al.*, 2006) and kindly gifted by the Department of Zoology, Trinity College Dublin. The CNA-35 probe is specific for type I and III collagen, found abundantly in skeletal muscle tissue. Following deparaffinisation, slides were prepared for a citrate buffer (pH 6) antigen retrieval step and subsequently stored in PBS (0.01M) prior to fluorescent staining. Slides were incubated over night at 4°C with CNA35-OG488 (1:100 dilution in PBS). Following staining, sliders were washed with PBS, incubated with Hoescht stain (Sigma-Aldrich) to visualize cell nuclei and finally cover slipped with PVA-DABCO mounting medium before observation with a confocal microscope (Leica SP8). Slides for immunohistochemistry were processed in parallel across all 4 groups and confocal image acquisition was performed with

standardized exposure settings, especially important for quantification of the relative area of collagen. *Data analysis*: For CNA35-OG488 analysis, non-overlapping serial images (x20 magnification) were taken across a whole diaphragm muscle section. Images were analysed using a colour balance threshold (ImageJ software), and the area of collagen was expressed as a percentage of the total area of muscle.

2.8 Molecular studies

2.8.1 Tissue preparation

Diaphragm samples stored at -80^{o}C were removed and allowed to defrost at 4^{o}C for 5 minutes. All procedures were performed at 4^{o}C to prevent protein degradation. Samples were homogenized in a lysis buffer (RIPA) made up from 10X RIPA, deionized water, 200mM sodium fluoride (NAF), 100mM phenylmethylsulfonylfluoride (PMSF), protease cocktail inhibitor 1 and phosphatase cocktail inhibitor 2. Following the homogenization process, the reactant mixtures were centrifuged (15,339 x *g*) at 4^{o}C for 20 min and the supernatants were harvested. The total amount of protein for each tissue sample was determined using the Pierce Bicinchoninic Acid Assay (BCA assay; Thermo Fisher Scientific, Dublin, Ireland). Supernatants were stored at -80^{o}C for subsequent use.

2.8.2 Cytokines

A multiplex cytokine assay (K15048G-1; Meso Scale Discovery, Rockville, MD) was used to examine cytokine concentrations in diaphragm muscle from all four groups (n = 8 per group). The assay was performed according to the manufacturer's instructions using an extended incubation time to improve detection (the plate was incubated overnight at 4^{o}C). Following incubation, the plate was read on a Quickplex SQ 120imager (Meso Scale Discovery). Values for each inflammatory mediator within each sample in each group (expressed at pg/ml) were above the lower limits of detection.

2.9 Statistical analysis

Data are expressed as scatter point box and whisker plots (median, 25-75 percentile, and scatter plot) or as mean ± S.D. Data were statistically compared using Prism 6.0 (Graphpad Software, San Diego,

CA, USA). For muscle immunohistochemistry and histology, group means were generated from multiple images averaged per animal. All data were statistically compared by two-way ANOVA (genotype x treatment) with Bonferroni post hoc test. $P < 0.05$ was deemed to be statistically significant. We have not reported statistical outcomes for WT+treatment compared with *mdx*+treatment throughout the text as this was not a focus of the study.

3. Results

Body mass and organ measurements

Table 1 compares body mass, body length, organ and muscle mass in WT and *mdx* mice treated with saline or xIL-6R and Ucn2 (treatment). Spleen mass was significantly increased in *mdx* + saline ($P < 0.0001$; two-way ANOVA with Bonferroni) compared with WT + saline. Muscle mass was significantly increased for *mdx* + saline tibialis anterior ($P < 0.0001$) and soleus ($P < 0.01$) compared with WT + saline. Extensor digitorum longus from *mdx* mice was significantly heavier than WT ($P = 0.001$ (genotype); two-way ANOVA). There was a significant difference in body mass ($P < 0.0001$ (genotype); two-way ANOVA) between age-matched WT and *mdx* mice; *mdx* mice were heavier. Drug co-treatment had no effect on body mass ($P = 0.411$ (treatment); two-way ANOVA). Spleen and muscle mass were also unaffected by drug treatment.

Baseline ventilation and metabolism

Respiratory flow traces for WT and *mdx* mice following saline or drug co-treatment are shown in Fig. 1A. Minute ventilation during normoxia was significantly lower in *mdx* + saline compared with WT + saline (Fig. 1B; $P < 0.01$; two-way ANOVA with Bonferroni). The reduction in normoxic ventilation was due to a significantly lower tidal volume in *mdx* + saline compared with WT + saline (Table 2; $P < 0.05$). Respiratory frequency was significantly greater in *mdx* mice (Table 2; $P = 0.0047$ (genotype); two-way ANOVA). Drug co-treatment in *mdx* mice significantly increased minute ventilation (Table 2 and Fig. 1B; $P < 0.001$; two-way ANOVA with Bonferroni), due to a significant increase in tidal volume (Table 2. $P < 0.05$; two-way ANOVA with Bonferroni) and respiratory frequency (Table 2; $P = 0.0018$ (treatment); two-way ANOVA). There was no evidence of altered respiratory variability in *mdx* + saline mice compared with WT + saline, based on measures of breathing variability (SD1 and SD2; Table 2). Moreover, drug co-treatment had no effect on SD1 or SD2 for both WT and *mdx* mice.

There was no difference in $\dot{V}O_2$ (Table 2; P = 0.4439 (genotype); two-way ANOVA) and $\dot{V}CO_2$ (Table 2 and Figure 1C.; P = 0.8405) between WT and *mdx*. Drug co-treatment significantly decreased $\dot{V}O_2$ (Table 2) and $\dot{V}CO_2$ (Table 2 and Fig. 1C) in WT ($P < 0.05$ and $P < 0.01$; two-way ANOVA with Bonferroni; $\dot{V}O_2$ and $\dot{V}CO_2$, respectively) and *mdx* mice ($P < 0.05$ and $P < 0.05$). The ventilatory equivalent for O_2 ($V_E/\dot{V}O_2$) was significantly increased in WT (Table 2; $P < 0.05$) and *mdx* mice ($P < 0.05$) following drug co-treatment. Similarly, the ventilatory equivalent for CO_2 ($V_E/\dot{V}CO_2$) was significantly increased by drug co-treatment for both WT (Table 2 and Fig. 1D; $P < 0.001$) and *mdx* mice (Fig. 1D; $P < 0.001$). Drug co-treatment had a significant effect on the ratio of $\dot{V}CO_2$ to $\dot{V}O_2$ (Table 2; P = 0.0344 (treatment); two-way ANOVA).

Ventilatory responsiveness to hypoxia

Respiratory flow traces for WT and *mdx* mice during hypoxia following saline or drug co-treatment are shown in Fig. 2A. Ventilation was significantly lower in *mdx* + saline compared with WT + saline when examined as maximum ventilation during hypoxic challenge (Fig. 2B; $P < 0.0001$). The peak ventilatory response to hypoxia (ΔV_E) was lower in *mdx* + saline compared with WT + saline (Fig. 2C; $P < 0.001$; two-way ANOVA with Bonferroni). Drug co-treatment significantly increased peak ventilation (Fig. 2B; P = 0.0006) for *mdx* + treatment compared with *mdx* + saline. However, the peak ventilatory response to hypoxia (ΔV_E) was unchanged in *mdx* + treatment compared with *mdx* + saline (Fig. 2C; $P > 0.05$). By comparison, in WT mice, drug co-treatment had no significant effect on peak ventilation in response to hypoxia (Fig. 2B; P = 0.716). $V_E/\dot{V}CO_2$ increased in response to hypoxia (Fig. 2D; $P < 0.0001$). Drug co-treatment significantly increased $V_E/\dot{V}CO_2$ during hypoxia in WT (P = 0.024) but not *mdx* mice (P = 0.268). Ventilation was significantly lower in *mdx* + saline compared with WT + saline during hypercapnic challenge (V_E during hypercapnia was 4.0 ± 1.4 *versus* 2.4 ± 0.8 ml/min/g, two-way ANOVA with Bonferroni *post hoc* test, $P < 0.001$ for WT + saline (n=8) *versus* *mdx* + saline (n=8)). The peak ventilatory response to hypercapnia (ΔV_E) was lower in *mdx* + saline compared with WT + saline (delta V_E was 2.9 ± 1.5 *versus* 1.4 ± 0.7 ml/min/g, unpaired Student's *t* test, P = 0.21 for WT + saline (n=8) *versus mdx* + saline (n=8)). We were unable to compare the effect of drug co-treatment on hypercapnic ventilation in WT and *mdx* mice.

Isometric force and twitch contractile kinetics

Table 3 shows data for diaphragm muscle contractile kinetics (CT and ½ RT) from WT and *mdx* mice following saline or drug co-treatment. Diaphragm CT was significantly higher for *mdx* + saline ($P < 0.05$; two-way ANOVA with Bonferroni) compared with WT + saline. Drug co-treatment had no significant effect on CT. There was no significant difference between WT and *mdx* for ½ RT. Representative original traces for diaphragm muscle twitch and tetanic contractions, and maximum unloaded shortening are shown in Fig. 3A-C. Diaphragm twitch force was significantly lower in *mdx* + saline (Fig. 3D; $P < 0.05$) compared with WT + saline. Drug co-treatment had no significant effect on diaphragm twitch force (Fig. 3D; $P = 0.1766$ (treatment); two-way ANOVA). Diaphragm peak tetanic force at 100 Hz was significantly lower in *mdx* + saline (Fig. 3E; $P < 0.001$; two-way ANOVA with Bonferroni) compared with WT + saline. *Post hoc* analysis showed that drug treatment significantly increased tetanic force in *mdx*, but not WT diaphragm (Fig. 3E; $P < 0.05$). The outcomes were equivalent when absolute diaphragm force was compared between groups.

Isotonic contractile parameters and kinetics

Table 3 shows data for diaphragm muscle isotonic contractile parameters: Wmax, Pmax, Smax and Vmax. Diaphragm Wmax was significantly reduced in *mdx* + saline compared with WT + saline ($P < 0.05$; two-way ANOVA with Bonferroni). There was no significant effect of drug co-treatment on Wmax ($P = 0.0857$ (treatment); two-way ANOVA). Pmax was significantly reduced in *mdx* + saline compared with WT + saline ($P < 0.05$; two-way ANOVA with Bonferroni). Drug treatment significantly increased Pmax ($P = 0.0276$ (treatment); two-way ANOVA); Pmax was increased by ~130% in *mdx* diaphragm following drug treatment. There was no significant difference in Smax or Vmax between WT and *mdx* diaphragms. Statistical significance was not achieved for the effect of drug co-treatment on Wmax and Vmax in *mdx* diaphragm, perhaps due to insufficient statistical power, but sizeable effects were noted, which may have physiological relevance. Drug co-treatment increased *mdx* diaphragm Wmax by ~100% and Vmax by ~58% compared with *mdx* + saline.

Isotonic load relationships

Figure 3 (F-I) shows data for diaphragm muscle isotonic load relationships. Loading had a significant effect on work (Fig. 3F; $P < 0.0001$; two-way ANOVA), power (Fig. 3G; $P < 0.0001$), shortening (Fig. 3H; $P < 0.0001$) and shortening velocity (Fig. 3I; $P < 0.0001$). Diaphragm from *mdx* + saline had significantly reduced work ($P < 0.0001$), power ($P < 0.0001$), shortening ($P < 0.0001$) and shortening velocity ($P = 0.0003$) compared with WT + saline. Drug treatment increased *mdx* diaphragm work ($P < 0.0001$) and WT diaphragm work ($P = 0.059$). Following drug co-treatment, power production was significantly increased in WT ($P = 0.009$) and *mdx* diaphragm ($P < 0.0001$). Shortening ($P = 0.0001$) and shortening velocity ($P < 0.0001$) were also significantly increased for *mdx* diaphragm after drug co-treatment.

Myosin heavy chain fibre-type distribution

Figure 4 shows data for MyHC fibre distribution of diaphragm muscles. Representative immunofluorescence images of diaphragm fibre-type distribution are shown in Fig. 4A. The fibre type distribution of MyHC type I fibres did not vary significantly between the four groups (Fig. 4B). For *mdx* + saline, the abundance of MyHC type IIa fibres was significantly increased compared with WT + saline (Fig. 4C; $P < 0.001$; two-way ANOVA with Bonferroni), whereas the abundance of MyHC type IIx fibres was significantly reduced in *mdx* + saline compared with WT + saline (Fig. 4D; $P < 0.001$). The abundance of MyHC type IIb fibres was significantly reduced in *mdx* compared with WT diaphragm (Fig. 4E; $P = 0.0079$ (genotype); two-way ANOVA). Diaphragm fibre type changes were prevented or reversed by drug co-treatment in *mdx* with a significant decrease in type IIa fibres ($P < 0.001$; two-way ANOVA with Bonferrroni) and a significant increase in type IIx fibres ($P < 0.001$) observed compared with *mdx* + saline.

Fibre cross-sectional area

Figure 4F shows data for CSA for all fibre types in all 4 groups. There was no significant difference in the CSA of MyHC type I, type IIa, type IIx or type IIb fibres in *mdx* diaphragm compared with WT. Drug co-treatment significantly increased MyHC type I fibre CSA ($P < 0.05$; two-way ANOVA

with Bonferroni) and MyHC type IIx fibre CSA ($P < 0.05$) in *mdx* mice only. Drug co-treatment had no effect on the CSA of MyHC type IIa or type IIb fibres in WT and *mdx* diaphragms.

Central nucleation and putative inflammatory cell infiltration

Figure 5 shows data for diaphragm muscle histology. Figure 5A-C shows representative histological images of diaphragm muscle transverse sections stained with Haematoxylin and Eosin (A), Masson's trichrome (B) and CNA35-OG488 (C). The proportion of diaphragm muscle fibres with centrally located nuclei was significantly increased in *mdx* + saline (Fig 5D; $P < 0.001$; two-way ANOVA with Bonferroni) compared with WT + saline. Drug co-treatment had no significant effect on central nucleation ($P = 0.414$ (treatment); two-way ANOVA). The areal density of inflammatory cell infiltration was significantly increased in *mdx* + saline diaphragm compared with WT + saline (Fig. 5E; $P < 0.001$; two-way ANOVA with Bonferroni). Drug co-treatment had no significant effect on the relative area of putative immune cell infiltration ($P = 0.3114$ (treatment); two-way ANOVA).

Collagen content

The areal density of collagen labelled using Masson's trichrome (type I collagen) staining was significantly increased in *mdx* + saline compared with WT + saline (Fig. 5F; $P < 0.0001$; two-way ANOVA with Bonferroni). Drug co-treatment had no significant effect on type I collagen content ($P = 0.278$ (treatment); two-way ANOVA). Type I and type III collagen co-expression, labelled with the fluorescent CNA35-OG488 probe, was significantly increased in *mdx* diaphragm compared with WT (Fig. 5G; $P = 0.0449$ (genotype); two-way ANOVA). Drug co-treatment did not affect the expression of diaphragm type I and III collagen ($P = 0.99$ (treatment); two-way ANOVA).

Inflammatory mediators

Figure 6 shows data for selective cytokine concentrations in diaphragm muscle from WT and *mdx* mice after saline administration or drug co-treatment. There was a significantly increased concentration of IL-1β (Fig. 6A; $P < 0.0001$ (genotype); two-way ANOVA), IL-2 (Fig. 6B; $P =$

0.001), IL-5 (Fig. 6D; $P = 0.002$), IL-6 (Fig. 6E; $P = 0.0003$), KC/GRO (Fig. 6H; $P < 0.0001$) and TNF-α (Fig. 6J; $P < 0.0001$) in *mdx* diaphragm compared with WT. *Post hoc* analysis revealed that diaphragms from *mdx* + saline showed significantly increased expression of IL-1β (Fig. 6A; $P < 0.001$; Bonferroni), IL-6 (Fig. 6E; $P < 0.001$), KC/GRO (Fig. 6H; $P < 0.001$) and TNF-α (Fig. 6J; $P < 0.001$) compared with WT + saline. Two-way ANOVA revealed that drug co-treatment significantly decreased IL-1β ($P = 0.005$) and significantly increased IL-10 ($P = 0.029$). *Post hoc* analysis revealed that drug co-treatment significantly decreased the pro-inflammatory cytokine IL-1β (Fig. 6A. $P < 0.01$; Bonferroni) and significantly increased the anti-inflammatory cytokine IL-10 (Fig. 6F; $P < 0.05$) in *mdx* diaphragm compared with *mdx* + saline. The expression of IL-4 (Fig. 6C), IL-12p70 (Fig. 6G) and IFN-γ (Fig. 6I) were unchanged in *mdx* diaphragm compared with WT, and the concentrations of each of these were unaffected by drug co-treatment. Fig. 6K shows a heat map summarising the fold-change of cytokines relative to the WT + saline group.

4. Discussion

The key findings of the present study are: (i) drug co-treatment with xIL-6R and Ucn2 restored *mdx* diaphragm muscle fibre complement equivalent to WT; (ii) drug co-treatment improved diaphragm force-generating capacity and restored normoxic ventilation in *mdx* mice; (iii) drug co-treatment had no significant effect on central nucleation, inflammatory cell infiltration and collagen deposition in *mdx* diaphragm; and (iv) drug co-treatment decreased IL-1β concentration and increased IL-10 concentration in *mdx* diaphragm.

Striated muscle weakness is a devastating result of dystrophin deficiency and associated pathology in DMD. Respiratory muscle function is compromised and boys with DMD have reduced ventilatory capacity, which declines with age (De Bruin *et al.*, 1997; Khirani *et al.*, 2014). Diaphragm muscle weakness and likely impaired performance of the upper airway musculature translates to sleep disordered breathing including obstructive sleep apnoea and hypoventilation in many boys with DMD (Smith *et al.*, 1989; Barbé *et al.*, 1994). Cardiorespiratory failure is the leading cause of death in DMD, thus treatment strategies aimed at improving and prolonging adequate cardio-respiratory function are necessary.

Diaphragm muscle weakness is well described in *mdx* mice from a young age (Coirault *et al.*, 2003). In the current study, diaphragm muscle from *mdx* + saline mice showed significantly reduced twitch force and increased contraction time compared with WT + saline. Similarly, peak tetanic force at 100Hz and maximum work- and power-generating capacity were significantly reduced for *mdx* + saline diaphragm compared with WT + saline. These data confirm previous findings illustrating mechanical dysfunction in the *mdx* diaphragm (Stedman *et al.*, 1991). We have previously reported depressed diaphragm force-generating capacity in *mdx* diaphragm at stimulation frequencies relevant to eupnoeic (basal) breathing (Burns *et al.*, 2017c). Although the principal inspiratory muscle is compromised in DMD and *mdx* mice, few studies have comprehensively examined respiratory function and ventilatory capacity in *mdx* mice, both important measures to consider when examining the effects of novel therapeutic strategies in animal models of myopathic disease.

In the current study, we assessed breathing in conscious unrestrained mice using whole-body plethysmography. Minute ventilation during normoxia was significantly reduced in *mdx* + saline compared with WT + saline mice, consistent with our recent reports (Burns *et al.*, 2015; Burns *et al.*, 2017c). The observed reductions in ventilation were the result of significant reductions in tidal volume in *mdx* mice. Although minute ventilation was lower in *mdx* mice, there was no difference in whole-body metabolism (as measured by $\dot{V}CO_2$) between age-matched saline-treated WT and *mdx* mice, consistent with recent data (Burns *et al.*, 2017c). Consequentially, $\dot{V}_E/\dot{V}_{CO2}$ was lower in *mdx* compared with WT (24±8 *versus* 18±5; mean±SD, WT *versus mdx)*, although this was not deemed statistically significant by *post hoc* analysis. Despite evidence of impaired normoxic ventilation in the *mdx* model, there is no apparent evidence of inherent respiratory instability based on the analysis of variability of inspiratory and expiratory durations in young *mdx* mice.

Ventilation was significantly blunted in *mdx* mice evidenced by decreased minute ventilation during hypoxic gas exposure. Drug co-treatment significantly increased hypoxic ventilation, consistent with recovery of mechanical deficits in *mdx* mice. Of note, the acute ventilatory response to hypoxia, measured as the absolute change in ventilation from baseline was blunted in *mdx* mice, a finding consistent with *mdx* carotid body hypoactivity (Burns *et al*., 2017c). Drug co-treatment did not reverse this effect suggesting that the sensory deficit is unrelated to IL-6-dependent and/or CRFR2-dependent signalling in the hypoxic chemoafferent pathway of *mdx* mice. $\dot{V}_E/\dot{V}CO_2$ was elevated during hypoxic

exposure revealing a hypoxic hyperventilation in WT and *mdx* mice. Drug co-treatment significantly increased V_E/VCO_2 during hypoxia in WT, but not in *mdx* mice.

Murine diaphragm muscle expresses MyHC type I, IIa, IIx and IIb fibres (Sieck *et al.*, 2012; Burns et al., 2017c). Diaphragm muscle weakness in *mdx* + saline diaphragm was associated with an alteration in the distribution of MyHC isoform composition, with *mdx* + saline diaphragm expressing fewer MyHC IIx fibres and more MyHC IIa fibres compared with WT + saline. MyHC type II fibres display an incremental increase in force production from IIa to IIx to IIb, respectively. Thus, a shift in MyHC composition from IIx to IIa in *mdx* diaphragm muscle fibres likely has functional implications, consistent with *mdx* diaphragm exhibiting lower force- and power-generating capacity *ex vivo*. Similar alterations in MyHC distribution have been reported in pharyngeal dilator muscles from *mdx* mice (Burns *et al.*, 2017b) and are likely due to ongoing muscle fibre damage and repair processes preventing muscle fibre MyHC isoform maturation during muscle development.

Mechanical dysfunction of striated muscle is coupled with extensive inflammation of the respiratory and non-respiratory musculature in DMD (Messina *et al.*, 2011) and *mdx* mice (Barros Maranhão *et al.*, 2015). Inflammation occurs due to muscle fibre damage as a result of dystrophin deficiency. Inflammatory cells are recruited to the damaged muscle to repair injured fibres. There is elevated expression of inflammatory cytokines in plasma and muscle biopsies from DMD boys (De Pasquale *et al.*, 2012; Cruz-Guzmán *et al.*, 2015) and *mdx* mice (Rufo *et al.*, 2011). Chronic immune activation and attendant inflammation, observed in DMD, can have detrimental effects on normal physiological function. During the years of ambulation, plasma cytokine levels appear to be near maximal in DMD boys and begin to decline thereafter when patients become non-ambulatory (Cruz-Guzmán *et al.*, 2015), perhaps due to the disuse of the lower limb musculature. IL-6 is one of many cytokines reported to be elevated in DMD (Rufo *et al.*, 2011; Cruz-Guzmán *et al.*, 2015; Pelosi *et al.*, 2015a) and is of particular relevance due to its role as a myokine and muscle signalling molecule. Plasma IL-6 is known to increase in response to intense exercise and in pathological diseases such as Crohn's disease and rheumatoid arthritis (Maggio *et al.*, 2006). IL-6 binds to the IL-6R which signals via the Janus kinase/signal transducer activator of transcription (JAK/STAT) pathway. IL-6 can have divergent actions on skeletal muscle signalling such as promoting both muscle growth and wasting. These opposing effects are consistent with the pro- and anti-inflammatory actions of IL-6. In some

cases, IL-6 has been linked with hypertrophic muscle growth and paradoxically linked to muscle atrophy and wasting (Muñoz-Cánoves *et al.*, 2013). These conflicting actions may relate to different concentration levels of IL-6 and acute *versus* persistent action of IL-6 signalling pathways.

The pro-inflammatory cytokines IL-1β, IL-6, KC/GRO and TNF-α were significantly increased in *mdx* + saline diaphragm muscle compared with WT + saline, indicating a pro-inflammatory signature, consistent with previous reports in *mdx* muscle (Porter *et al.*, 2002). This elevated expression of inflammatory cytokines was associated with a significant increase in the percent infiltration of putative inflammatory cells in *mdx* + saline diaphragm compared with WT + saline. The number of muscle fibres expressing central nuclei in *mdx* + saline diaphragm was also elevated compared with WT + saline, indicating muscle fibre repair and regeneration. Blockade of IL-6 signalling in *mdx* mice has been shown to improve the capacity for treadmill exercise (Pelosi *et al.*, 2015a), to normalize function of gastrointestinal smooth muscle (Manning *et al.*, 2016), and exert modest effects on improving diaphragm force (Manning *et al.*, 2017). Conversely, overexpression of IL-6 in *mdx* mice promotes muscle necrosis and satellite cell exhaustion (Pelosi *et al.*, 2015b). Blockade of IL-6 signalling in dystrophin-/utrophin-deficient mice ameliorated skeletal muscle damage and promoted muscle regeneration in the limb, but no beneficial effects were observed for cardiac and respiratory muscle (Wada *et al.*, 2017).

Muscle wasting and proteolysis are pathophysiological features of myopathies such as DMD. Corticosteroids have been the treatment of choice for many years in DMD, notwithstanding their unwanted side effects (Ricotti *et al.*, 2013). Therapies aimed at activating anabolic signalling in functional muscle fibres may act to improve muscle force in DMD and *mdx* mice. The urocortins which bind to the CRFRs are known to modulate muscle mass and anabolic signalling pathways in skeletal muscle (Hinkle *et al.*, 2003a). Upon activation of CRFR2, there is an increase in adenylyl cyclase and cAMP formation (Reutenauer-Patte *et al.*, 2012). Skeletal muscle is known to express CRFR2, and activation of CRFR2 decreased nerve damage and corticosteroid- and disuse-induced skeletal muscle mass and function loss in mice, and increased muscle mass in non-atrophying muscle (Hinkle *et al.*, 2003b). The CRFR2 agonist, Ucn2, has been shown to improve diaphragm muscle force (Hinkle *et al.*, 2007; Manning *et al.*, 2017), increase muscle mass (Hall *et al.*, 2007) and decrease muscle damage (Reutenauer-Patte *et al.*, 2012) in *mdx* mice.

In the current study, we investigated the effects of IL-6R blockade (xIL-6R) and CRFR2 agonism (Ucn2) on ventilation and metabolism and diaphragm muscle structure, function and cytokine concentration. Blocking the action of IL-6 was performed using a neutralizing IL-6R monoclonal antibody (Okazaki *et al.*, 2002). Intervention began at a relatively young age (six weeks) and was performed for a 2 week duration. Breathing and diaphragm muscle assessments were performed following treatment at eight weeks of age. Recent findings from our group have shown this treatment strategy to improve diaphragm force-generating capacity (Manning *et al.*, 2017) and to restore pharyngeal dilator muscle force in *mdx* mice (Burns *et al.*, 2017b). In the latter study, the observed improvements in *mdx* pharyngeal dilator muscle function was associated with significantly reduced central nucleation of sternohyoid muscle from *mdx* mice following drug co-treatment (Burns *et al.*, 2017a).

Co-treatment of xIL-6R and Ucn2 significantly increased diaphragm specific force in *mdx* + treatment compared with saline-treated *mdx* (9±3 *versus* 16±3 N/cm^2; mean±SD, *mdx* + saline *versus mdx* + treatment). For isotonic load relationships, drug co-treatment significantly increased diaphragm work, power, shortening and shortening velocity for *mdx* diaphragm. These findings confirm and extend previous data describing improved muscle force following administration of xIL-6R and Ucn2 in *mdx* diaphragm (Manning *et al.*, 2017) and upper airway muscle (Burns *et al.*, 2017b). Of interest, enhanced force-generating capacity in WT diaphragm was not observed following co-treatment with xIL-6R and Ucn2.

Diaphragm muscle MyHC composition was significantly altered following xIL-6R and Ucn2 co-treatment in *mdx* mice. Drug co-treatment significantly reduced MyHC type IIa and increased MyHC type IIx fibre distribution in *mdx* diaphragm compared with saline treated *mdx* mice. Improved *mdx* diaphragm force-generating capacity following drug co-treatment may be due to preservation of MyHC type IIx fibres. Drug co-treatment in WT mice had no effect on diaphragm fibre type distribution compared with saline-treated WT, consistent with no change in force-generating capacity in WT diaphragm. Progression of *mdx* diaphragm muscle fibres from MyHC IIa to IIx may be due, at least in part, to a suppression of muscle fibre damage and thus maturation of muscle fibres. The

findings are consistent with previous observations in sternohyoid muscle from *mdx* mice following the same therapeutic intervention (Burns *et al.*, 2017b). In addition to preservation of MyHC fibre type distribution, drug co-treatment promoted hypertrophy (increased CSA) of MyHC type I and IIx fibres in *mdx* diaphragm which likely translates to functional improvements, since muscle force-generating capacity is proportional to fibre cross-sectional area. The observed hypertrophy of MyHC type I and IIx fibres may be a result of altered anabolic signalling mediated by Ucn2 in *mdx* mice. Drug co-treatment had no effect on muscle fibre central nucleation indicating there were no apparent improvements in muscle fibre damage and repair processes. Moreover, collagen content was also unaffected by drug co-treatment. These data suggest that functional improvements observed in the *mdx* diaphragm are not as a result of improvements in muscle damage and fibrosis, but are rather likely due to effects on healthy muscle fibres. Of interest however, if the beneficial effects of drug co-treatment relate to a positive inotropic effect on healthy fibres in *mdx* muscle, it appears unique to *mdx* since drug co-treatment did not increase WT diaphragm force.

Enhanced diaphragm functional capacity and altered MyHC isoform composition following drug co-treatment in *mdx* mice, was associated with significantly increased tidal volume and minute ventilation during normoxia compared with saline-treated *mdx*. Both tidal volume and minute ventilation, which were decreased in *mdx* + saline compared to WT + saline, were restored to WT + saline values in *mdx* mice following co-treatment. Indices of metabolism, V_{O2} and V_{CO2} were significantly reduced by drug co-treatment in WT and *mdx* compared with saline controls. The ventilatory equivalents for O_2 and CO_2 were both significantly increased by drug treatment in WT and *mdx* compared with saline-treated controls. Drug co-treatment had no effect on the variability of breathing in WT and *mdx* mice showing no overt effects of xIL-6R and Ucn2 on respiratory stability. The mechanism of the hypometabolic effect of drug co-treatment is unclear and warrants attention in future studies.

Interestingly, drug co-treatment significantly decreased IL-1β concentration in *mdx* diaphragm, with a concomitant increase in the concentration of the anti-inflammatory cytokine, IL-10. These data suggest modest improvements in the pro/anti-inflammatory cytokine balance in *mdx* diaphragm. There was no significant effect of drug co-treatment on the relative area of the putative inflammatory cell infiltration. Blockade of IL-6 signalling with xIL-6R did not significantly affect IL-6

concentration in *mdx* diaphragm muscle. Drug co-treatment in WT and *mdx* mice had no effect on body mass, indices of somatic growth and muscle and organ mass, demonstrating no apparent adverse effects of the drug co-treatment at their respective doses for the two-week duration of the current intervention.

Limitations

We used the *mdx* mouse model in our studies and compared findings to a separate age-matched inbred colony (BL10), which served as control. This study design is consistent with the general approach in the *mdx* literature and consistent with recent reports (Terrill *et al*., 2016; Whitehead *et al*., 2016; Burns et al., 2017c; Pinniger *et al*., 2017). A breeding strategy to generate mixed littermates who differ only in the absence or presence of dystrophin (Bellinger *et al*., 2009) would represent a refinement of our approach and should be considered by researchers into the future. Such strategies are commonplace in studies of genetically modified mice and rats. It is possible that the *mdx* phenotype that we describe is exaggerated compared with WT BL10 mice, because of an inbred mutation in the WT mice associated with gain of function, or perhaps more likely that the WT values for at least some variables are also impaired in the inbred WT mice due to one or more mutations leading to loss of function, which would lead to an under-representation of the dystrophin-deficient *mdx* phenotype, and perhaps confounders in the comparisons between *mdx* and BL10. Arguing against this point however, values for BL10 diaphragm force in this study compare well with the published literature for other mouse strains, and this was confirmed by us in the present study by assessment of age-matched male C57/BL6 diaphragm force (peak force = 21±4 N/cm^2, mean±SD, n=3), which was equivalent to peak diaphragm force in C57/BL10. Moreover, this is generally consistent with previously published data from our group using adult male C57/BL6 mice (O'Leary & O'Halloran 2016; O'Leary *et al*., 2018). We have previously performed ventilatory measures in C57/BL6 mice (O'Leary & O'Halloran 2016; O'Leary *et al*., 2018) and these values are similar to BL10 data reported by us (Burns *et al*., 2017c; present study) and the wider literature in other strains. Cross-breeding of *mdx* with C57/BL6 to generate mixed genotype litters has been described in *mdx* studies (Bellinger *et al*., 2009), but it is important to consider that BL6 mice may not be a suitable background strain for ventilatory studies in dystrophin-deficient mice since BL6 mice express intrinsic respiratory instability and central apneas (Strohl, 2003). The issue of potential genetic drift in inbred control BL10 mice from a separate colony obviously does not have relevance to the *mdx* values

that we report herein, which compare well with the published literature. Moreover, the primary focus of our study was examination of the effect of drug intervention on *mdx* muscle strength, quality and breathing, which is independent of any concerns that might be expressed in respect of the most appropriate control group for our study.

It is important to acknowledge that muscle injury in *mdx* dystrophic muscle triggers a cascade of degeneration, regeneration, inflammation, oxidative stress and progressive damage, as seen in human DMD, such that physiological and pathophysiological traits at different time points in the disease, and models of it, may be reflective of the underlying processes at play *per se* inasmuch as they are of dystrophin deficiency. We see no conflict in the fact that the *mdx* model expresses complex physiological and pathophysiological responses in muscle (and nervous control of muscle) triggered by dystrophin lack, which may be recapitulated by other stressors (e.g. oxidative stress). As is the case in DMD, the weakened muscle is a reflection of a devastating combination of aberrant factors such that the explicit impact of dystrophin lack *per se* cannot easily be determined. There are several other mouse models of muscular dystrophy, for example D2-*mdx* (Coley *et al*., 2016) and *mdx*4cv/mTRG2 (Yucel *et al*., 2018), which purportedly better recapitulate the human dystrophinopathies at least for limb and cardiac muscle. However, whether this also applies to the respiratory muscles and their control is much less clear. There are very distinct differences in the pathology of diaphragm and limb muscles in *mdx*. Since there is a paucity of information on the control of breathing in *mdx* mice (and essentially all other models), there is no way yet to know how different models compare and whether one particular model is optimal for studies of diaphragm function and breathing. It is important to emphasize that diaphragm force loss is substantial even at 8 weeks of age in *mdx* providing a useful model for the interventional study that we performed. Nevertheless, we acknowledge the need to confirm our findings in other models of muscular dystrophy, particularly if our study is to have translational value to DMD.

Ventilatory capacity in *mdx* mice was assessed by whole-body plethysmography in conscious animals, which provides an estimate of tidal volume with known limitations (Mortola & Frappell, 1998; Burns *et al.*, 2017c). We employed hypoxic gas challenges to increase ventilation, but this provides only a modest ventilatory challenge, especially in mice, which adopt a hypometabolic strategy in response to hypoxia, such that the increase in minute ventilation is relatively small. We assessed hypercapnic

breathing, which revealed a clear deficit in *mdx* compared with WT, but again the activation of the diaphragm required to increase ventilation in response to chemostimulation is modest. As such, we did not assess the full range of ventilatory capacity (and deficit) in *mdx* mice and the efficacy of drug co-treatment in restoring physiological function associated with high levels of diaphragm and accessory muscle activation. Peak diaphragm force-generating capacity was determined in *ex vivo* preparations in this study. Assessment of respiratory muscle function *in situ*, such as measurements of transdiaphragmatic pressure (Greising *et al.*, 2013) and assessment of peak inspiratory pressure-generating capacity in mice across a range of ventilatory and non-ventilatory behaviours would be useful in characterizing the magnitude of the mechanical deficit in *mdx* mice at 8 weeks of age, and the efficacy or otherwise of drug co-treatment in the preservation of ventilatory capacity.

We acknowledge that our intervention strategy was relatively short-lived and applied at one early time point in a murine model of a progressive disease. In the future, drug co-treatment for longer durations and at different stages of disease progression across various models of DMD are necessary to fully explore the capacity for this novel intervention to influence muscle quality and strength, including the potential for deleterious outcomes or side effects with long-term drug treatment. Moreover, whereas the restoration of diaphragm strength and ventilation was impressive in our study, we concede that drug intervention did not affect muscle necrosis and fibrosis, and did not reduce the area of immune cell infiltrate in muscle tissue, although the explicit cellular nature of the infiltrate was not explored in this study. As such, the improvements in muscle function appear to relate to actions on healthy fibres in *mdx* muscle, which has implications in the context of translation of this interventional strategy to DMD patients.

Summary & Conclusion

In summary, *mdx* mice have impaired ventilation, diaphragm muscle weakness and MyHC fibre-type immaturity at an early age. Co-treatment with xIL-6R antibodies and Ucn2 recovered *mdx* diaphragm force-generating capacity. Drug co-treatment preserved the MyHC fibre complement in *mdx* diaphragm and also promoted hypertrophy of MyHC type I and IIx fibres in *mdx* but not WT diaphragm. Preservation and hypertrophy of *mdx* diaphragm muscle MyHC type IIx fibres may be adequate for functional improvements, especially since drug co-treatment did not influence measures

of necrosis, fibrosis and immune cell infiltration in *mdx* diaphragm, suggesting actions on healthy fibres, although interestingly no inotropic effect of drug co-treatment was evident in WT muscle. Normoxic ventilation was recovered in *mdx* drug-treated mice, mediated by restoration of tidal volume. Combined drug treatment led to improvements in diaphragm MyHC composition and force-generating capacity, associated with improved ventilatory capacity in young *mdx* mice. These findings have relevance to the development of interventional therapies for human dystrophinopathies.

5. References

Barbé F, Quera-Salva MA, McCann C, Gajdos P, Raphael JC, de Lattre J & Agustí AG (1994). Sleep-related respiratory disturbances in patients with Duchenne muscular dystrophy. *Eur Respir J* **7,** 1403-1408.

Barros Maranhão J, de Oliveira Moreira D, Maurício AF, de Carvalho SC, Ferretti R, Pereira JA, Santo Neto H & Marques MJ (2015). Changes in calsequestrin, TNF-α, TGF-β and MyoD levels during the progression of skeletal muscle dystrophy in mdx mice: a comparative analysis of the quadriceps, diaphragm and intrinsic laryngeal muscles. *Int J Exp Pathol* **96,** 285-293.

Bellinger AM, Reiken S, Carlson C, Mongillo M, Liu X, Rothman L, Matecki S, Lacampagne A & Marks AR (2009). Hypernitrosylated ryanodine receptor calcium release channels are leaky in dystrophic muscle. *Nat Med*. **15**, 325-30.

Blake DJ, Weir A, Newey SE & Davies KE (2002). Function and genetics of dystrophin and dystrophin-related proteins in muscle. *Physiol Rev* **82,** 291-329.

Burns DP, Ali I, Rieux C, Healy J, Jasionek G & O'Halloran KD (2017a). Tempol Supplementation Restores Diaphragm Force and Metabolic Enzyme Activities in mdx Mice. *Antioxidants (Basel)* **6**.

Burns DP, Edge D, O'Malley D & O'Halloran KD (2015). Respiratory Control in the mdx Mouse Model of Duchenne Muscular Dystrophy. *Adv Exp Med Biol* **860,** 239-244.

Burns DP & O'Halloran KD (2016). Evidence of hypoxic tolerance in weak upper airway muscle from young mdx mice. *Respir Physiol Neurobiol* **226,** 68-75.

Burns DP, Rowland J, Canavan L, Murphy KH, Brannock M, O'Malley D, O'Halloran KD & Edge D (2017b). Restoration of pharyngeal dilator muscle force in dystrophin-deficient (mdx) mice following co-treatment with neutralizing interleukin-6 receptor antibodies and urocortin 2. *Exp Physiol* **102,** 1177-1193.

Burns DP, Roy A, Lucking EF, McDonald FB, Gray S, Wilson RJ, Edge D & O'Halloran KD (2017c). Sensorimotor control of breathing in the mdx mouse model of Duchenne muscular dystrophy. *J Physiol* **595,** 6653-6672.

Chahbouni M, Escames G, Venegas C, Sevilla B, García JA, López LC, Muñoz-Hoyos A, Molina-Carballo A & Acuña-Castroviejo D (2010). Melatonin treatment normalizes plasma pro-inflammatory cytokines and nitrosative/oxidative stress in patients suffering from Duchenne muscular dystrophy. *J Pineal Res* **48,** 282-289.

Coirault C, Lambert F, Marchand-Adam S, Attal P, Chemla D & Lecarpentier Y (1999). Myosin molecular motor dysfunction in dystrophic mouse diaphragm. *Am J Physiol* **277,** C1170-1176.

Coirault C, Pignol B, Cooper RN, Butler-Browne G, Chabrier PE & Lecarpentier Y (2003). Severe muscle dysfunction precedes collagen tissue proliferation in mdx mouse diaphragm. *J Appl Physiol (1985)* **94,** 1744-1750.

Coley WD, Bogdanik L, Vila MC, Yu Q, Van Der Meulen JH, Rayavarapu S, Novak JS, Nearing M, Quinn JL, Saunders A, Dolan C, Andrews W, Lammert C, Austin A, Partridge TA, Cox GA, Lutz C & Nagaraju K. Effect of genetic background on the dystrophic phenotype in mdx mice. *Hum Mol Genet*. **25**, 130-145.

Cruz-Guzmán OeR, Rodríguez-Cruz M & Escobar Cedillo RE (2015). Systemic Inflammation in Duchenne Muscular Dystrophy: Association with Muscle Function and Nutritional Status. *Biomed Res Int* **2015,** 891972.

De Bruin PF, Ueki J, Bush A, Khan Y, Watson A & Pride NB (1997). Diaphragm thickness and inspiratory strength in patients with Duchenne muscular dystrophy. *Thorax* **52,** 472-475.

De Paepe B & De Bleecker JL (2013). Cytokines and chemokines as regulators of skeletal muscle inflammation: presenting the case of Duchenne muscular dystrophy. *Mediators Inflamm* **2013,** 540370.

De Pasquale L, D'Amico A, Verardo M, Petrini S, Bertini E & De Benedetti F (2012). Increased muscle expression of interleukin-17 in Duchenne muscular dystrophy. *Neurology* **78,** 1309-1314.

Deconinck N & Dan B (2007). Pathophysiology of duchenne muscular dystrophy: current hypotheses. *Pediatr Neurol* **36,** 1-7.

Greising SM, Sieck DC, Sieck GC & Mantilla CB (2013). Novel method for transdiaphragmatic pressure measurements in mice. *Respir Physiol Neurobiol* **188,** 56-59.

Grundy D (2015). Principles and standards for reporting animal experiments in The Journal of Physiology and Experimental Physiology. *J Physiol*. **593**, 2547-2549.

Hall JE, Kaczor JJ, Hettinga BP, Isfort RJ & Tarnopolsky MA (2007). Effects of a CRF2R agonist and exercise on mdx and wildtype skeletal muscle. *Muscle Nerve* **36,** 336-341.

Haouzi P, Bell HJ, Notet V & Bihain B (2009). Comparison of the metabolic and ventilatory response to hypoxia and H2S in unsedated mice and rats. *Respir Physiol Neurobiol* **167,** 316-322.

Hinkle RT, Donnelly E, Cody DB, Bauer MB & Isfort RJ (2003a). Urocortin II treatment reduces skeletal muscle mass and function loss during atrophy and increases nonatrophying skeletal muscle mass and function. *Endocrinology* **144,** 4939-4946.

Hinkle RT, Donnelly E, Cody DB, Bauer MB, Sheldon RJ & Isfort RJ (2004). Corticotropin releasing factor 2 receptor agonists reduce the denervation-induced loss of rat skeletal muscle mass and force and increase non-atrophying skeletal muscle mass and force. *J Muscle Res Cell Motil* **25,** 539-547.

Hinkle RT, Donnelly E, Cody DB, Samuelsson S, Lange JS, Bauer MB, Tarnopolsky M, Sheldon RJ, Coste SC, Tobar E, Stenzel-Poore MP & Isfort RJ (2003b). Activation of the CRF 2 receptor modulates skeletal muscle mass under physiological and pathological conditions. *Am J Physiol Endocrinol Metab* **285,** E889-898.

Hinkle RT, Lefever FR, Dolan ET, Reichart DL, Dietrich JA, Gropp KE, Thacker RI, Demuth JP, Stevens PJ, Qu XA, Varbanov AR, Wang F & Isfort RJ (2007). Corticortophin releasing factor 2 receptor agonist treatment significantly slows disease progression in mdx mice. *BMC Med* **5,** 18.

Khan Y & Heckmatt JZ (1994). Obstructive apnoeas in Duchenne muscular dystrophy. *Thorax* **49,** 157-161.

Khirani S, Ramirez A, Aubertin G, Boulé M, Chemouny C, Forin V & Fauroux B (2014). Respiratory muscle decline in Duchenne muscular dystrophy. *Pediatr Pulmonol* **49,** 473-481.

Krahn KN, Bouten CV, van Tuijl S, van Zandvoort MA & Merkx M (2006). Fluorescently labeled collagen binding proteins allow specific visualization of collagen in tissues and live cell culture. *Anal Biochem* **350,** 177-185.

Lewis P, Sheehan D, Soares R, Coelho AV & O'Halloran KD (2016). Redox Remodeling Is Pivotal in Murine Diaphragm Muscle Adaptation to Chronic Sustained Hypoxia. *Am J Respir Cell Mol Biol* **55,** 12-23.

Lewis P, Sheehan D, Soares R, Varela Coelho A & O'Halloran KD (2015). Chronic sustained hypoxia-induced redox remodeling causes contractile dysfunction in mouse sternohyoid muscle. *Front Physiol* **6,** 122.

Maggio M, Guralnik JM, Longo DL & Ferrucci L (2006). Interleukin-6 in aging and chronic disease: a magnificent pathway. *J Gerontol A Biol Sci Med Sci* **61,** 575-584.

Manning J, Buckley MM, O'Halloran KD & O'Malley D (2016). In vivo neutralization of IL-6 receptors ameliorates gastrointestinal dysfunction in dystrophin-deficient mdx mice. *Neurogastroenterol Motil* **28,** 1016-1026.

Manning J, Buckley MM, O'Halloran KD & O'Malley D (2017). Combined xIL-6R and urocortin-2 treatment restores mdx diaphragm muscle force. *Muscle Nerve*. **56**, E134-E140.

Messina S, Vita GL, Aguennouz M, Sframeli M, Romeo S, Rodolico C & Vita G (2011). Activation of NF-kappaB pathway in Duchenne muscular dystrophy: relation to age. *Acta Myol* **30,** 16-23.

Mortola JP & Frappell PB (1998). On the barometric method for measurements of ventilation, and its use in small animals. *Can J Physiol Pharmacol* **76,** 937-944.

Mosqueira M, Baby SM, Lahiri S & Khurana TS (2013). Ventilatory chemosensory drive is blunted in the mdx mouse model of Duchenne Muscular Dystrophy (DMD). *PLoS One* **8,** e69567.

Muñoz-Cánoves P, Scheele C, Pedersen BK & Serrano AL (2013). Interleukin-6 myokine signaling in skeletal muscle: a double-edged sword? *FEBS J* **280,** 4131-4148.

O'Halloran KD (2006). Effects of nicotine on rat sternohyoid muscle contractile properties. *Respir Physiol Neurobiol* **150,** 200-210.

O'Leary AJ & O'Halloran KD (2016). Diaphragm muscle weakness and increased UCP-3 gene expression following acute hypoxic stress in the mouse. *Respir Physiol Neurobiol* **226,** 76-80.

O'Leary AJ, Drummond SE, Edge D, O'Halloran KD (2018). Diaphragm muscle weakness following acute sustained hypoxic stress in the mouse is prevented by pretreatment with N-acetyl cysteine. *Oxid Med Cell Longev*. **19**, 2018:4805493.

Okazaki M, Yamada Y, Nishimoto N, Yoshizaki K & Mihara M (2002). Characterization of anti-mouse interleukin-6 receptor antibody. *Immunol Lett* **84,** 231-240.

Pelosi L, Berardinelli MG, De Pasquale L, Nicoletti C, D'Amico A, Carvello F, Moneta GM, Catizone A, Bertini E, De Benedetti F & Musarò A (2015a). Functional and Morphological Improvement of Dystrophic Muscle by Interleukin 6 Receptor Blockade. *EBioMedicine* **2,** 285-293.

Pelosi L, Berardinelli MG, Forcina L, Spelta E, Rizzuto E, Nicoletti C, Camilli C, Testa E, Catizone A, De Benedetti F & Musarò A (2015b). Increased levels of interleukin-6 exacerbate the dystrophic phenotype in mdx mice. *Hum Mol Genet* **24,** 6041-6053.

Peng YJ, Nanduri J, Khan SA, Yuan G, Wang N, Kinsman B, Vaddi DR, Kumar GK, Garcia JA, Semenza GL & Prabhakar NR (2011). Hypoxia-inducible factor 2α (HIF-2α) heterozygous-null mice exhibit exaggerated carotid body sensitivity to hypoxia, breathing instability, and hypertension. *Proc Natl Acad Sci U S A* **108,** 3065-3070.

Pinniger GJ, Terrill JR, Assan EB, Grounds MD & Arthur PG (2017). Pre-clinical evaluation of N-acetylcysteine reveals side effects in the mdx mouse model of Duchenne muscular dystrophy. *J Physiol*. **595**, 7093-7107.

Porter JD, Khanna S, Kaminski HJ, Rao JS, Merriam AP, Richmonds CR, Leahy P, Li J, Guo W & Andrade FH (2002). A chronic inflammatory response dominates the skeletal muscle molecular signature in dystrophin-deficient mdx mice. *Hum Mol Genet* **11,** 263-272.

Reutenauer-Patte J, Boittin FX, Patthey-Vuadens O, Ruegg UT & Dorchies OM (2012). Urocortins improve dystrophic skeletal muscle structure and function through both PKA- and Epac-dependent pathways. *Am J Pathol* **180,** 749-762.

Ricotti V, Ridout DA, Scott E, Quinlivan R, Robb SA, Manzur AY, Muntoni F & Network NC (2013). Long-term benefits and adverse effects of intermittent versus daily glucocorticoids in boys with Duchenne muscular dystrophy. *J Neurol Neurosurg Psychiatry* **84,** 698-705.

Rufo A, Del Fattore A, Capulli M, Carvello F, De Pasquale L, Ferrari S, Pierroz D, Morandi L, De Simone M, Rucci N, Bertini E, Bianchi ML, De Benedetti F & Teti A (2011). Mechanisms inducing low bone density in Duchenne muscular dystrophy in mice and humans. *J Bone Miner Res* **26,** 1891-1903.

Sieck DC, Zhan WZ, Fang YH, Ermilov LG, Sieck GC & Mantilla CB (2012). Structure-activity relationships in rodent diaphragm muscle fibers vs. neuromuscular junctions. *Respir Physiol Neurobiol* **180,** 88-96.

Smith PE, Calverley PM & Edwards RH (1988). Hypoxemia during sleep in Duchenne muscular dystrophy. *Am Rev Respir Dis* **137,** 884-888.

Smith PE, Edwards RH & Calverley PM (1989). Ventilation and breathing pattern during sleep in Duchenne muscular dystrophy. *Chest* **96,** 1346-1351.

Souza GM, Bonagamba LG, Amorim MR, Moraes DJ & Machado BH (2015). Cardiovascular and respiratory responses to chronic intermittent hypoxia in adult female rats. *Exp Physiol* **100,** 249-258.

Stedman HH, Sweeney HL, Shrager JB, Maguire HC, Panettieri RA, Petrof B, Narusawa M, Leferovich JM, Sladky JT & Kelly AM (1991). The mdx mouse diaphragm reproduces the degenerative changes of Duchenne muscular dystrophy. *Nature* **352,** 536-539.

Stirrat CG, Venkatasubramanian S, Pawade T, Mitchell AJ, Shah AS, Lang NN & Newby DE (2016). Cardiovascular effects of urocortin 2 and urocortin 3 in patients with chronic heart failure. *Br J Clin Pharmacol* **82,** 974-982.

Strohl KP (2003). Periodic breathing and genetics. *Respir Physiol Neurobiol*. **135**, 179-185.

Terrill JR, Pinniger GJ, Graves JA, Grounds MD & Arthur PG (2016). Increasing taurine intake and taurine synthesis improves skeletal muscle function in the mdx mouse model for Duchenne muscular dystrophy. *J Physiol*. **594**, 3095-3110.

Wada E, Tanihata J, Iwamura A, Takeda S, Hayashi YK & Matsuda R (2017). Treatment with the anti-IL-6 receptor antibody attenuates muscular dystrophy via promoting skeletal muscle regeneration in dystrophin-/utrophin-deficient mice. *Skelet Muscle* **7,** 23.

Whitehead NP, Bible KL, Kim MJ, Odom GL, Adams ME & Froehner SC (2016). Validation of ultrasonography for non-invasive assessment of diaphragm function in muscular dystrophy. *J Physiol*. **594**, 7215-7227.

Williams R, Lemaire P, Lewis P, McDonald FB, Lucking E, Hogan S, Sheehan D, Healy V & O'Halloran KD (2015). Chronic intermittent hypoxia increases rat sternohyoid muscle NADPH oxidase expression with attendant modest oxidative stress. *Front Physiol* **6,** 15.

Yucel N, Chang AC, Day JW, Rosenthal N & Blau HM (2018). Humanizing the mdx mouse model of DMD: the long and the short of it. *NPJ Regen Med*. **3**, 4.

6. Additional information

Funding

DPB was supported by funding from the Department of Physiology, UCC. Work carried out in TCD was supported by funding from the Department of Physiology, TCD. The monoclonal anti-IL-6 receptor antibody was gifted by Chugai Pharmaceuticals, Tokyo, Japan. We are grateful to staff of the Biological Services Unit, UCC for support with animal care and welfare. We are grateful to Dr. G. Jasionek, Department of Physiology, UCC for technical support.

Disclosures

The authors have no financial, professional or personal conflicts relating to this publication.

Author contributions

DPB: experimental design; acquisition of data; analysis and interpretation of data; drafting of the original manuscript; LC: acquisition of data; analysis; JR: acquisition of data; analysis; RO'F: acquisition of data; analysis; MB: acquisition of data; analysis; SED: acquisition of data; DO'M: experimental design; critical revision of the manuscript for important intellectual content; DE: experimental design; data acquisition; interpretation of data; drafting and critical revision of the manuscript for important intellectual content; KDO'H: experimental design; interpretation of data; drafting and critical revision of the manuscript for important intellectual content.

Figure legends

Figure 1. Ventilation in conscious mice during normoxia

A, representative respiratory flow traces during normoxia (21% O_2) in wild-type (WT) and *mdx* mice following six subcutaneous injections with saline (S; 0.9% w/v) or treatment [T; neutralizing interleukin-6 receptor antibodies (0.2 mg/kg) and urocortin 2 (30 µg/kg); co-administered] over 2 weeks. Inspiration downwards. B-D, minute ventilation (B), carbon dioxide production (C; $\dot{V}CO_2$) and ventilatory equivalent for carbon dioxide (D; $\dot{V}_E/\dot{V}CO_2$) for WT and *mdx* mice following saline or drug treatment. Values (B-D) are expressed as scatter point box and whisker plots (median, 25-75 percentile and scatter plot). Data were statistically compared by two-way ANOVA with Bonferroni *post hoc* test. $^{**}P < 0.01$; $^{***}P < 0.001$.

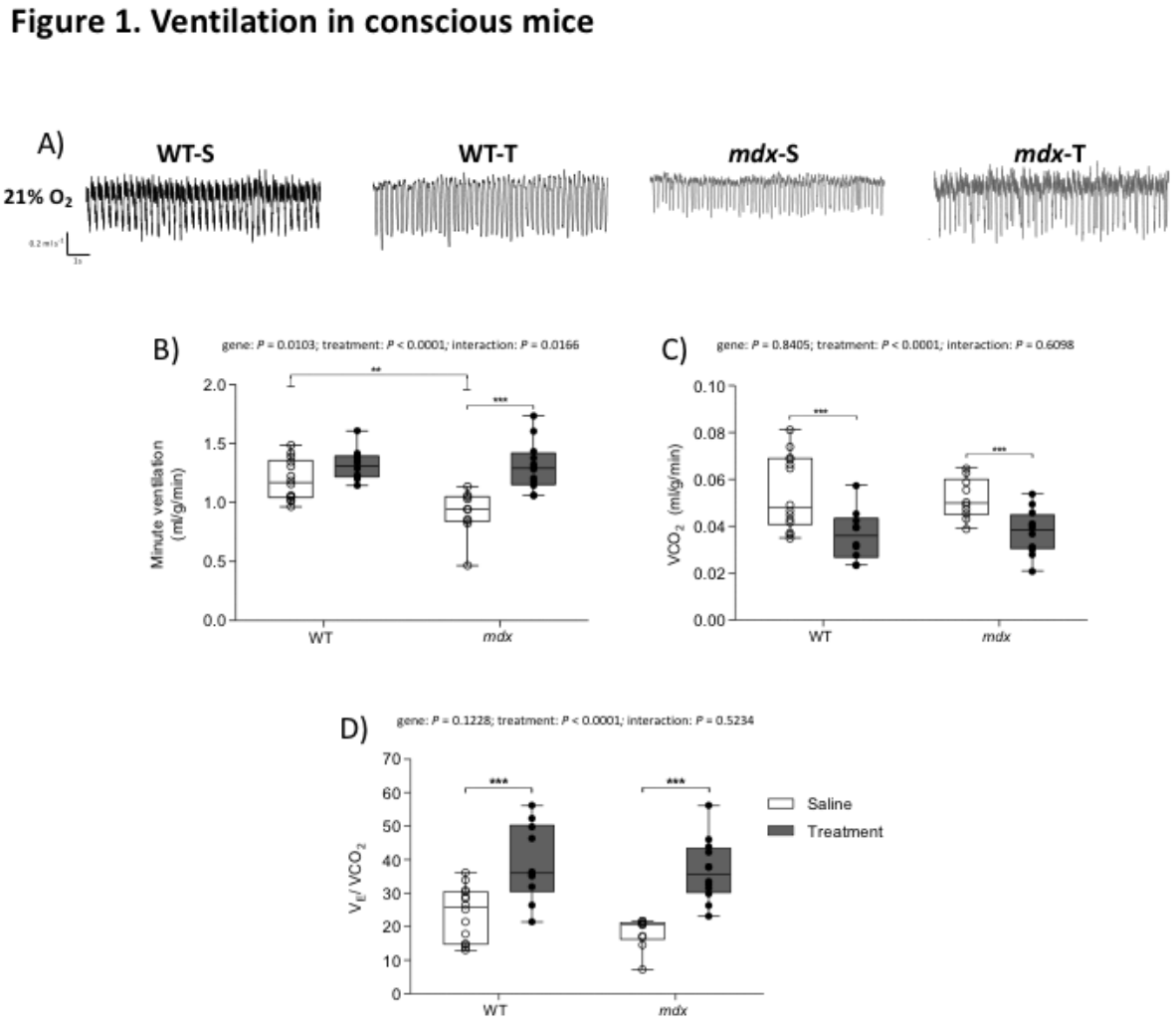

Figure 2. Ventilatory responsiveness to hypoxia

A, representative respiratory flow traces during hypoxia (10% O_2) in wild-type (WT) and *mdx* mice following six subcutaneous injections with saline (S; 0.9% w/v) or treatment [T; neutralizing interleukin-6 receptor antibodies (0.2 mg/kg) and urocortin 2 (30 μg/kg); co-administered] over 2 weeks. Inspiration downwards. B, Group data (mean ± SD) for minute ventilation during baseline and peak ventilation during hypoxia for WT and *mdx* mice following saline or drug treatment. Data were statistically compared by repeated measures two-way ANOVA. C, Group data for peak ventilatory responsiveness (ΔV_E) to hypoxia for WT and *mdx* mice following saline or drug treatment. Values are expressed as scatter point box and whisker plots (median, 25-75 percentile and scatter plot). Data were statistically compared by two-way ANOVA with Bonferroni *post hoc* test. *$P < 0.05$; ***$P < 0.001$. D, group data (mean ± SD) for ventilatory equivalent for carbon dioxide (V_E/VCO_2) during baseline and after 5-20 min of exposure to hypoxia for WT and *mdx* mice following saline or drug treatment. Data were statistically compared by repeated measures two-way ANOVA.

Figure 2. Ventilatory responsiveness to hypoxia

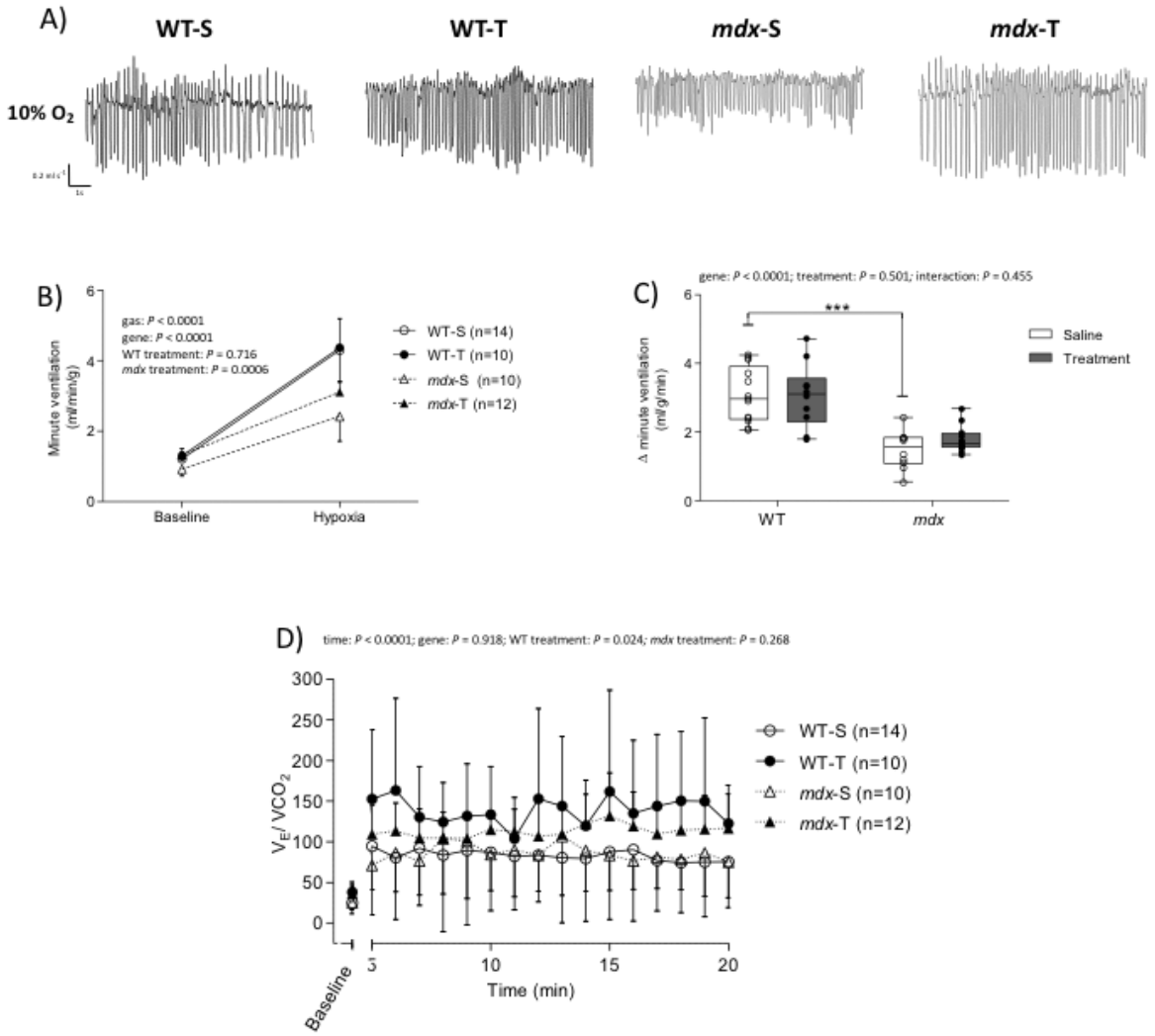

Figure 3. Diaphragm muscle function

A-C, original traces of muscle twitch (A) and tetanic (B) contractions and maximum unloaded shortening (C) for diaphragm muscle from wild-type (WT) and *mdx* mice following six subcutaneous injections with saline (S; 0.9% w/v) or treatment [T; neutralizing interleukin-6 receptor antibodies (0.2 mg/kg) and urocortin 2 (30 μg/kg); co-administered] over 2 weeks. D and E, group data for twitch (D) and tetanic (E) force in WT (n = 7-10) and *mdx* (n = 8) diaphragm muscle following saline or treatment. Peak tetanic force was measured following stimulation at 100Hz *ex vivo*. Values are expressed as scatter point box and whisker plots (median, 25-75 percentile and scatter plot). Data

were statistically compared by two-way ANOVA followed by Bonferroni *post hoc* test. *$P < 0.05$; ***$P < 0.001$. F-I, group data (mean ± SD) for work-load (F), power-load (G), shortening-load (H) and velocity-load (I) relationships in WT (n = 7-10) and *mdx* (n = 8) diaphragm muscle following saline or drug treatment. Data were statistically compared by two-way ANOVA.

Work: load, $P < 0.0001$; genotype, $P < 0.0001$; WT treatment, $P = 0.059$; and *mdx* treatment, $P < 0.0001$.

Power: load, $P < 0.0001$; genotype, $P < 0.0001$; WT treatment, $P = 0.009$; and *mdx* treatment, $P < 0.0001$.

Shortening: load, $P < 0.0001$; genotype, $P < 0.0001$; WT treatment, $P = 0.968$; and *mdx* treatment, $P = 0.0001$.

Velocity: load, $P < 0.0001$; genotype, $P = 0.0003$; WT treatment, $P = 0.642$; and *mdx* treatment, $P < 0.0001$.

Figure 3. Diaphragm muscle function

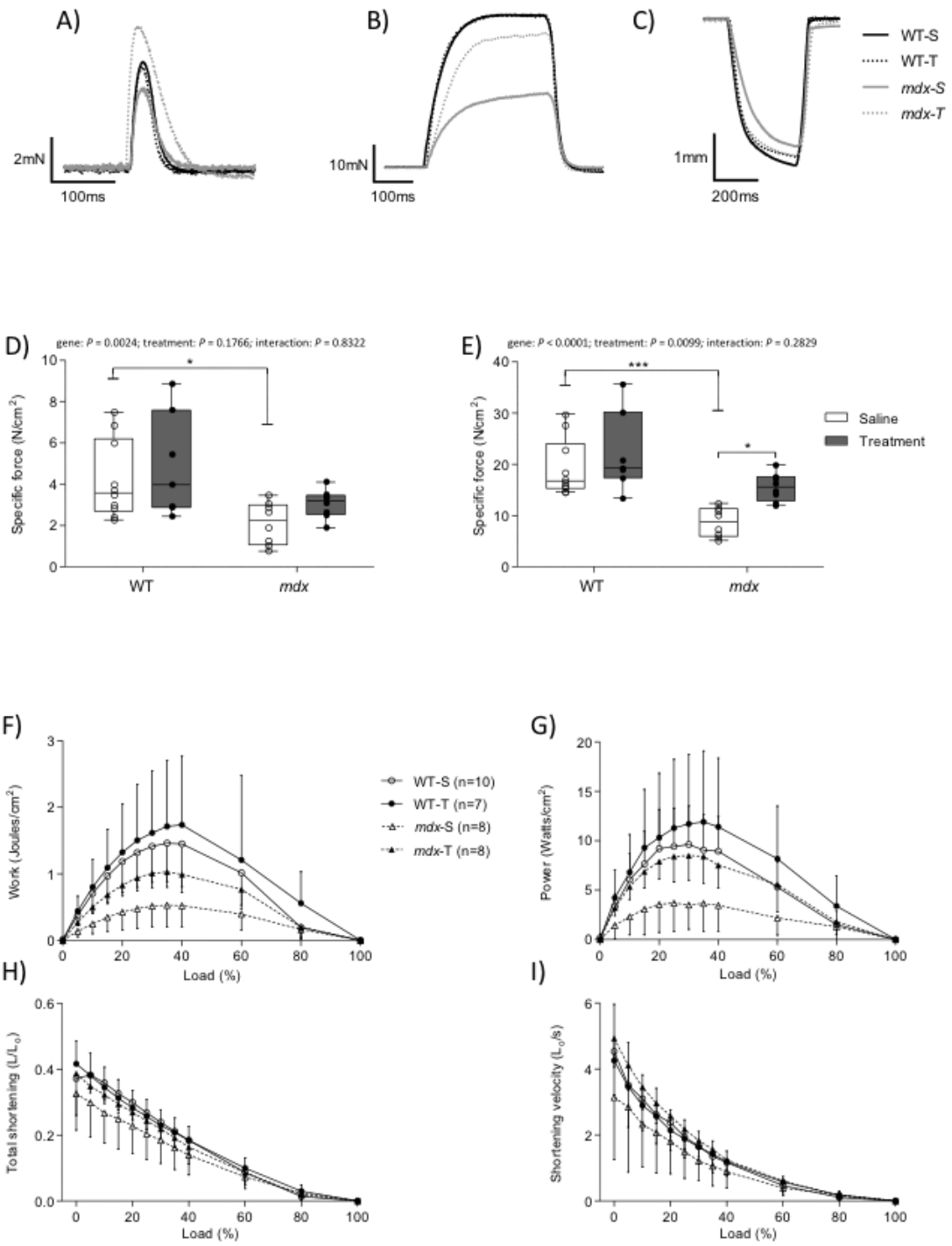

Figure 4. Diaphragm muscle fibre distribution and cross-sectional area (CSA)

A, Representative immunofluorescence images of diaphragm muscle fibre-type distribution (A), showing type I (blue), type IIa (red), type IIx (untagged, appearing black) and type IIb fibres (green) for WT + saline (WT-S; top left), *mdx* + saline (*mdx*-S; top right), WT + treatment (WT-T; bottom left) and *mdx* + treatment (*mdx*-T; bottom right). Scale bars = 200 μm. B-E, group data showing fibre distribution of type I (B), type IIa (C), type IIx (D) and type IIb fibres (E) in WT and *mdx* saline treated mice, and WT drug-treated and *mdx* drug-treated mice (n=5) per group. Mice received six sub-cutaneous injections of saline (0.9% w/v) or treatment [neutralizing interleukin-6 receptor antibodies (0.2 mg/kg) and urocortin 2 (30 μg/kg); co-administered] over two weeks. Values are expressed as scatter point box and whisker plots (median, 25-75 percentile and scatter plot). Data were statistically compared by two-way ANOVA followed by Bonferroni *post hoc* test. ***$P < 0.001$. F, Group data (mean ± SD) showing mean CSAs of diaphragm muscle fibre type I, type IIa, type IIx and type IIb. Data were statistically analysed by two-way ANOVA with Bonferroni *post hoc* test. *$P < 0.01$.

Type I: Genotype, $P = 0.908$; treatment, $P = 0.036$; interaction, $P = 0.009$.
Type IIa: Genotype, $P = 0.839$; treatment, $P = 0.291$; interaction, $P = 0.27$.
Type IIx: Genotype, $P = 0.276$; treatment, $P = 0.005$; interaction, $P = 0.106$.
Type IIb: Genotype, $P = 0.12$; treatment, $P = 0.905$; interaction, $P = 0.281$.

Figure 4. Diaphragm muscle fibre distribution and cross-sectional area (CSA)

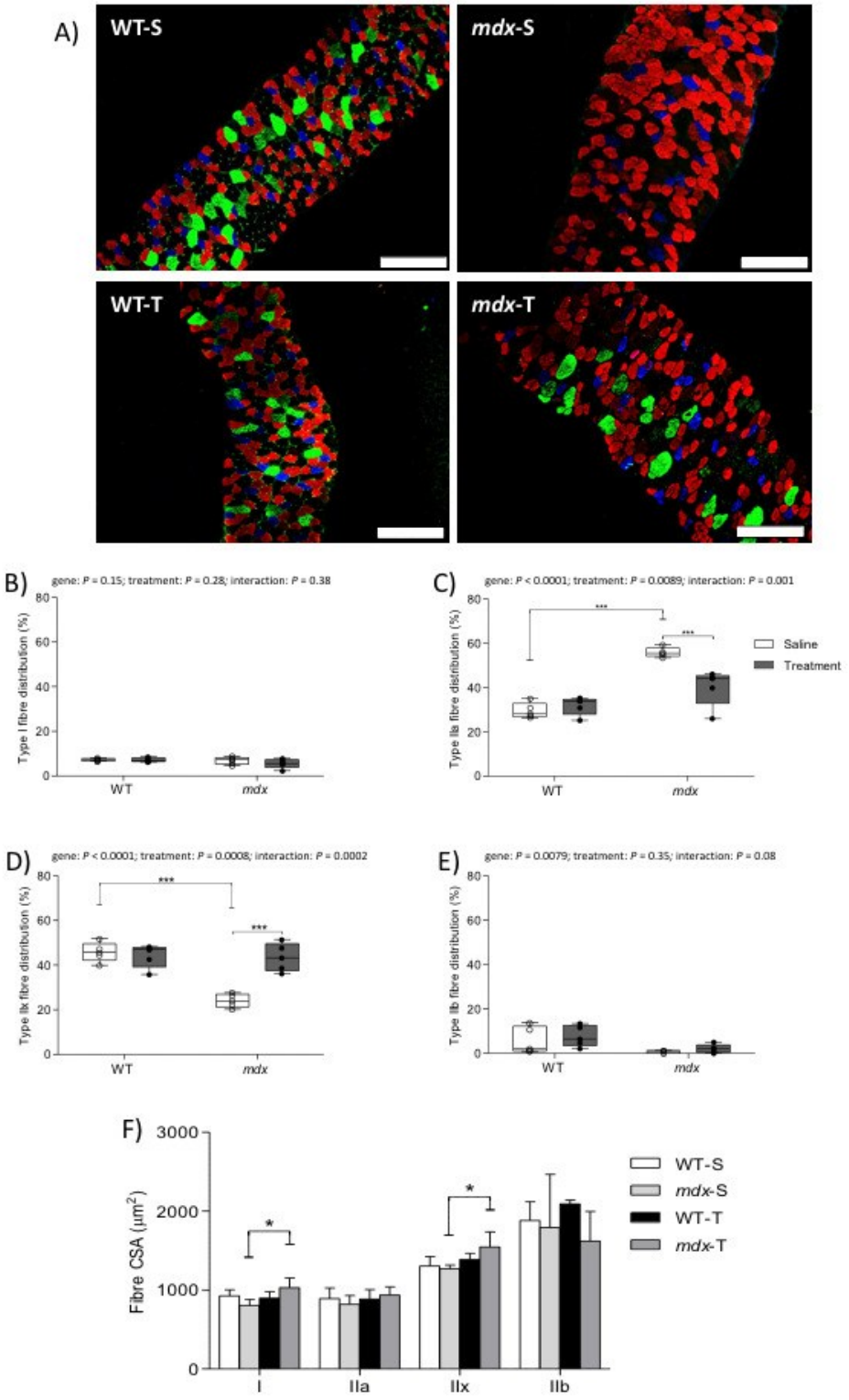

Figure 5. Diaphragm muscle histology

A-C, Representative histological images of diaphragm muscle transverse sections stained with Haematoxylin and Eosin (A), Masson's trichrome (B; type I collagen) and CNA35-OG488 (C; type I and III collagen) in WT + saline (WT-S; first column), *mdx* + saline (*mdx*-S; second column), WT + treatment (WT-T; third column) and *mdx* + treatment (*mdx*-T; fourth column) groups. Scale bars represent 100 μm. Peripherally located nuclei are apparent in WT saline and WT drug-treated images. In comparison, *mdx* mice (saline and drug-treated) displayed an increased incidence of centrally located nuclei. Inflammatory cell infiltration is not apparent in WT saline and WT drug-treated groups. The *mdx* muscle (saline and treatment) displayed inflammatory cell infiltration, highlighted with black arrows. D and E, group data showing the percentage of central nucleation (D) and percentage of infiltration of inflammatory cells (E) in diaphragm muscle from saline-treated WT (n = 5) and saline-treated *mdx* mice (n = 4), and WT (n = 5) and *mdx* (n = 5) mice treated with neutralizing interleukin-6 receptor antibodies (0.2 mg/kg) and urocortin 2 (30 μg/kg), co-administered as six sub-cutaneous injections over 2 weeks. F and G, group data showing percentage of type I collagen content (C) and type I and III collagen content (D) in diaphragm muscle from saline-treated WT and saline-treated *mdx* mice, and WT and *mdx* mice (n = 4-5 per group) treated with neutralizing interleukin-6 receptor antibodies (0.2 mg/kg) and urocortin 2 (30 μg/kg) co-administered as six sub-cutaneous injections over 2 weeks. Values are expressed as scatter point box and whisker plots (median, 25-75 percentile and scatter plot). Data were statistically compared by two-way ANOVA followed by Bonferroni *post hoc* test. ***$P <$ 0.001.

Figure 5. Diaphragm muscle histology

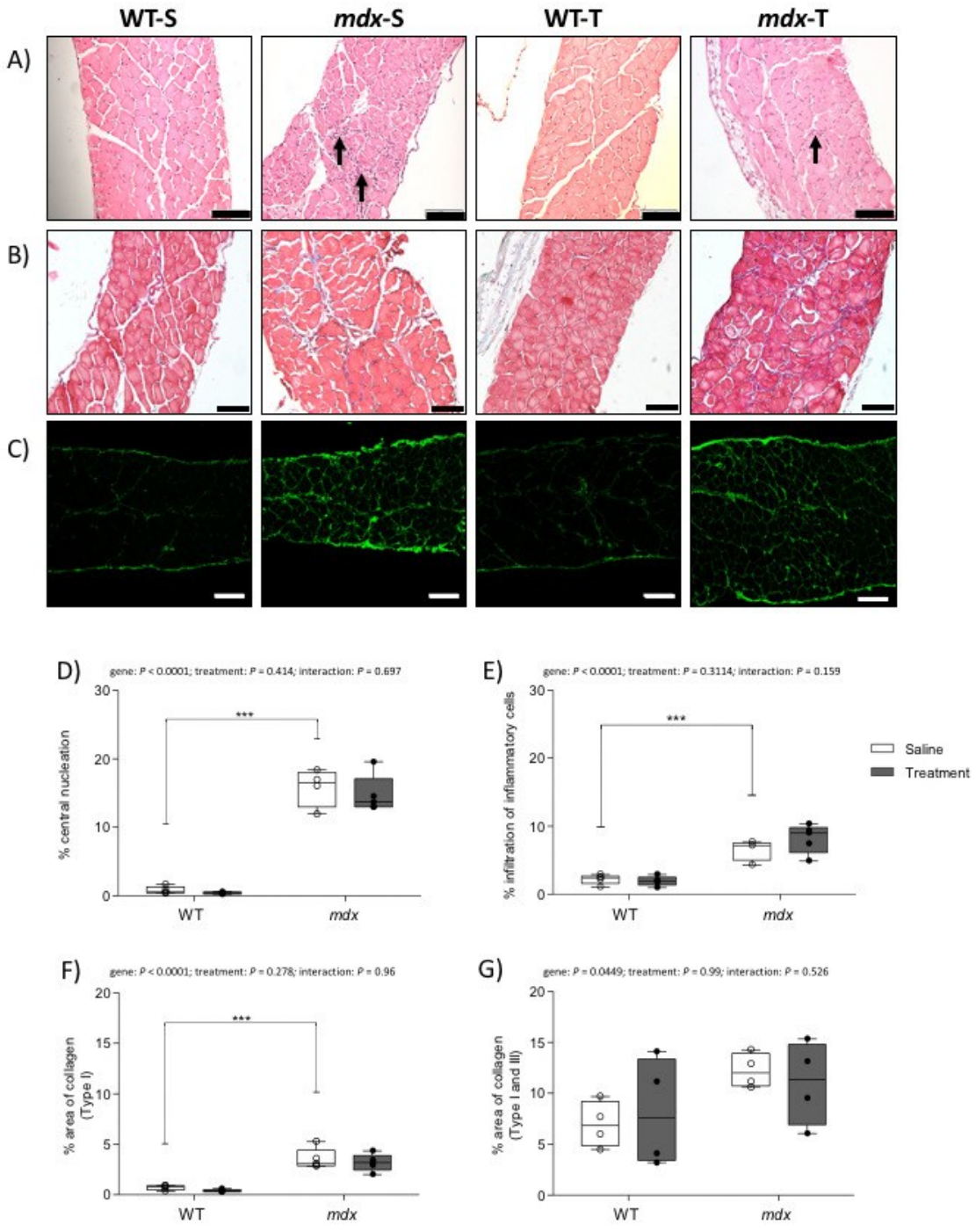

Figure 6. Cytokine concentrations in diaphragm muscle.

A-J, Group data (mean ± S.D) for selective cytokine concentrations in diaphragm muscle. Cytokines include interleukin-1β (A; IL-1β), interleukin-2 (B; IL-2), interleukin-4 (C; IL-4), interleukin-5 (D; IL-5), interleukin-6 (E; IL-6), interleukin-10 (F; IL-10); interleukin-12 (F; IL-12p70), (G; KC/GRO), interferon-γ (F; IFN- γ) and tumour necrosis factor-α (TNF-α) in diaphragm muscle from wild-type (WT) and *mdx* mice (n = 8 per group) injected subcutaneously with saline (S; 0.9% w/v) or drug treatment [T; neutralizing interleukin-6 receptor antibodies (0.2 mg/kg) and urocortin 2 (30 μg/kg); co-administered] over 2 weeks. K, Heat map illustrating fold-change in cytokine concentration relative to the WT + saline group. Red represents an increase in concentration. Data were statistically compared by two-way ANOVA followed by Bonferroni *post hoc* test. * $P < 0.05$; ** $P < 0.01$; *** $P < 0.001$.

Figure 6. Cytokine concentrations in diaphragm muscle

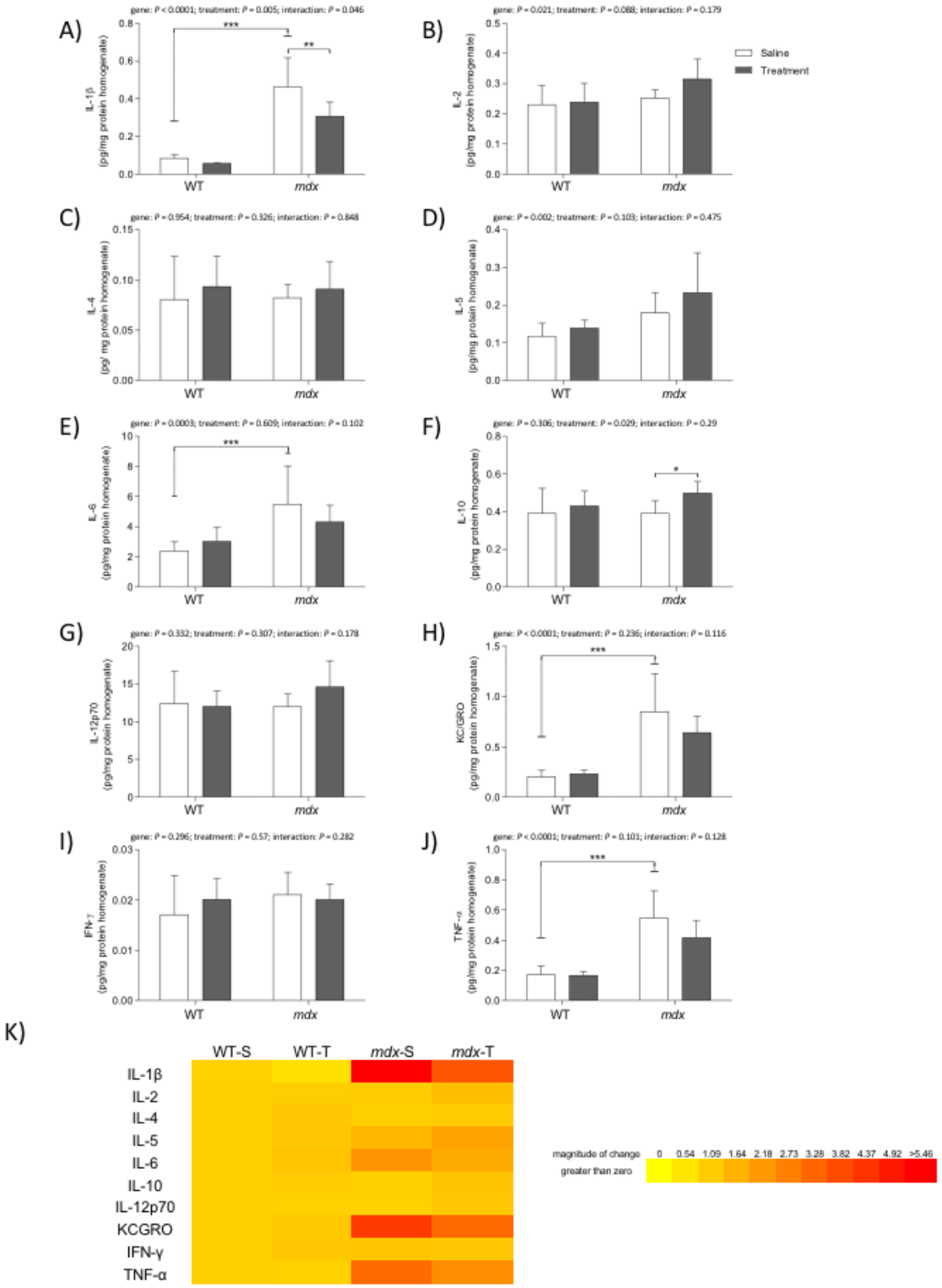

Table legends

Table 1. Body mass, somatic growth, organ and muscle mass

Definition of abbreviations: N-A, distance from nose to anus; N-T, distance from nose to tip of tail; RV, right heart ventricle; LV, left heart ventricle; TA, tibialis anterior; EDL, extensor digitorum longus; sol, soleus; WT, wild-type. WT (n = 7-10) and *mdx* (n = 6-10) mice were injected subcutaneously with saline (0.9% w/v) or treatment [neutralizing interleukin-6 receptor antibodies (0.2 mg/kg) and urocortin 2 (30 µg/kg); co-administered] over 2 weeks. Data are shown as mean ± SD and were statistically compared using two-way ANOVA with Bonferroni *post hoc* test. **mdx* saline significantly different from corresponding WT saline values, $P < 0.05$.

	WT		*mdx*		
	Saline (n = 10)	**Treatment (n = 7)**	**Saline (n = 10)**	**Treatment (n = 6)**	**Two-way ANOVA**
Body mass (g)	21.0 ± 1.3	21.6 ± 0.8	24.4 ± 1.7*	24.7 ± 1.6	Genotype: $P < 0.0001$; Treatment: $P = 0.411$; Interaction: $P = 0.7638$
N-A (cm)	9.1 ± 0.2	9.2 ± 0.3	9.4 ± 0.2	9.1 ± 0.3	Genotype: $P = 0.2576$; Treatment: $P = 0.2576$; Interaction: $P = 0.0121$
N-T (cm)	16.5 ± 0.3	16.8 ± 0.4	16.6 ± 0.3	16.8 ± 0.4	Genotype: $P = 0.4746$; Treatment: $P = 0.038$; Interaction: $P = 0.549$
Spleen (mg)	55.8 ± 8.9	60.6 ± 6.2	119.4 ± 13.5*	118.8 ± 23.3	Genotype: $P < 0.0001$; Treatment: $P = 0.6693$; Interaction: $P = 0.5816$
Wet lung (mg)	124.5 ± 10.2	113.7 ± 7.5	121.8 ± 9.0	124.0 ± 9.4	Genotype: $P = 0.2576$; Treatment: $P = 0.1966$; Interaction: $P = 0.0556$
Heart (mg)	103.1 ± 8.1	96.7 ± 7.6	106.0 ± 10.1	110.1 ± 11.0	Genotype: $P = 0.0167$; Treatment: $P = 0.7295$; Interaction: $P = 0.1112$
RV (mg)	25.8 ± 5.3	30.9 ± 3.5	31.5 ± 5.3	31.7 ± 6.8	Genotype: $P = 0.1073$; Treatment: $P = 0.1821$; Interaction: $P = 0.2172$
LV (mg)	77.4 ± 7.6	68.5 ± 7.1	74.5 ± 7.1	78.5 ± 8.4	Genotype: $P = 0.2028$; Treatment: $P = 0.3757$; Interaction: $P = 0.027$

RV:LV	0.34 ± 0.09	0.46 ± 0.09	0.42 ± 0.07	0.41 ± 0.09	Genotype: $P = 0.5691$; Treatment: $P = 0.105$; Interaction: $P = 0.0354$
TA (mg)	34.7 ± 2.5	35.7 ± 1.5	58.4 ± 3.4*	70.0 ± 4.8	Genotype: $P < 0.0001$; Treatment: $P = 0.1363$; Interaction: $P = 0.5224$
EDL (mg)	7.6 ± 2.2	6.2 ± 1.5	9.1 ± 1.8	9.2 ± 0.6	Genotype: $P = 0.001$; Treatment: $P = 0.2852$; Interaction: $P = 0.266$
Sol (mg)	5.9 ± 1.3	6.0 ± 1.2	8.5 ± 1.7*	8.7 ± 1.9	Genotype: $P < 0.0001$; Treatment: $P = 0.7927$; Interaction: $P = 0.9906$

Table 2. Baseline ventilation and metabolic measurements

Definition of abbreviations: f_R, breathing frequency; V_T, tidal volume; V_E, minute ventilation; VO_2, oxygen consumption; VCO_2, carbon dioxide production; V_E/VO_2, ventilatory equivalent for oxygen; V_E/VCO_2, ventilatory equivalent for carbon dioxide; VCO_2/VO_2, respiratory exchange ratio; Ti, inspiratory duration; Te, expiratory duration; SD1, short-term variability; SD2, long-term variability; WT, wild-type. WT (n = 10-14) and *mdx* (n = 10-12) mice were injected subcutaneously with saline (0.9% w/v) or treatment [neutralizing interleukin-6 receptor antibodies (0.2 mg/kg) and urocortin 2 (30 µg/kg); co-administered] over 2 weeks. Data are shown as mean ± SD and were statistically compared using two-way ANOVA with Bonferroni *post hoc* test. ‡WT treatment significantly different from corresponding WT saline values, $P < 0.05$; **mdx* saline significantly different from corresponding WT saline values, $P < 0.05$; #*mdx* treatment significantly different from corresponding *mdx* saline values, $P < 0.05$.

	WT		***mdx***		
	Saline (n = 14)	**Treatment (n = 10)**	**Saline (n = 10)**	**Treatment (n = 12)**	**Two-way ANOVA**
f_R (bpm)	165.0 ± 11.2	177.7 ± 11.9‡	176.4 ± 15.7	189.0 ± 12.7	Genotype: $P = 0.0047$; Treatment: $P = 0.0018$; Interaction: $P = 0.977$
V_T (ml/g)	0.0074 ± 0.001	0.0076 ± 0.001	0.0053 ± 0.001*	0.0071 ± 0.001#	Genotype: $P < 0.0001$; Treatment: $P = 0.0016$; Interaction: $P = 0.017$
V_E (ml/g/min)	1.19 ± 0.17	1.32 ± 0.13	0.92 ± 0.19*	1.31 ± 0.21#	Genotype: $P = 0.0103$; Treatment: $P < 0.0001$; Interaction: $P = 0.0166$
VO_2 (ml/g/min)	0.065 ± 0.02	0.037 ± 0.01‡	0.068 ± 0.02	0.043 ± 0.02#	Genotype: $P = 0.4439$; Treatment: $P < 0.0001$; Interaction: $P = 0.7139$

$\dot{V}CO_2$ (ml/g/min)	0.054 ± 0.02	0.036 ± 0.01[‡]	0.052 ± 0.01	0.038 ± 0.01[#]	Genotype: $P = 0.8405$; Treatment: $P < 0.0001$; Interaction: $P = 0.6089$
$V_E/\dot{V}O_2$	21.9 ± 11.7	38.3 ± 10.6[‡]	14.6 ± 5.1	35.5 ± 14.3[#]	Genotype: $P = 0.1344$; Treatment: $P < 0.0001$; Interaction: $P = 0.5089$
$V_E/\dot{V}CO_2$	23.9 ± 8.0	39.1 ± 18.2[‡]	18.2 ± 4.6	36.7 ± 9.3[#]	Genotype: $P = 0.1228$; Treatment: $P < 0.0001$; Interaction: $P = 0.5234$
$\dot{V}CO_2/\dot{V}O_2$	0.85 ± 0.2	1.03 ± 0.3	0.80 ± 0.2	0.97 ± 0.3	Genotype: $P = 0.4647$; Treatment: $P = 0.0344$; Interaction: $P = 0.9504$
Ti: SD1	18.9 ± 18.2	22.0 ± 8.6	16.3 ± 8.7	14.0 ± 5.0	Genotype: $P = 0.128$; Treatment: $P = 0.9128$; Interaction: $P = 0.432$
Ti: SD2	27.2 ± 14.0	28.1 ± 9.9	26.2 ± 21.1	21.0 ± 5.8	Genotype: $P = 0.3048$; Treatment: $P = 0.579$; Interaction: $P = 0.4387$
Te: SD1	59.8 ± 34.7	59.1 ± 26.0	63. 7 ± 36.7	45.5 ± 17.6	Genotype: $P = 0.5739$; Treatment: $P = 0.2777$; Interaction: $P = 0.3155$
Te: SD2	93.1 ± 41.0	79.5 ± 19.6	75.6 ± 49.9	60.9 ± 19.5	Genotype: $P = 0.0888$; Treatment: $P = 0.1827$; Interaction: $P = 0.9323$

Table 3. Diaphragm muscle contractile properties

Group data (mean ± SD) for twitch contraction time (CT), twitch half-relaxation time (1/2 RT), maximum mechanical work (Wmax), maximum mechanical power (Pmax), peak shortening (Smax) and peak shortening velocity (Vmax) of diaphragm muscle from wild-type (WT; n = 7-10) and *mdx* (n = 8) mice injected subcutaneously with saline (0.9% w/v) or treatment [neutralizing interleukin-6 receptor antibodies (0.2 mg/kg) and urocortin 2 (30 µg/kg); co-administered] over 2 weeks. Data were statistically compared by two-way ANOVA followed by Bonferroni *post hoc* test. **mdx* saline significantly different from corresponding WT saline value, $P < 0.05$.

	WT		*mdx*		
	Saline (n = 10)	**Treatment (n = 7)**	**Saline (n = 8)**	**Treatment (n = 8)**	**Two-way ANOVA**
CT (ms)	18.4 ± 2.8	19.4 ± 2.1	21.8 ± 2.5*	21.6 ± 2.5	Genotype *P* = 0.0038; Treatment *P* = 0.6824; Interaction *P* = 0.5097
½ RT (ms)	23.5 ± 2.2	22.3 ± 2.6	23.9 ± 1.2	21.2 ± 6.4	Genotype *P* = 0.8129; Treatment *P* = 0.1353; Interaction *P* = 0.5761
Wmax (J/cm^2)	1.5 ± 0.7	1.7 ± 1.0	0.5 ± 0.3*	1.0 ± 0.1	Genotype *P* = 0.0008; Treatment *P* = 0.0857; Interaction *P* = 0.6102
Pmax (W/cm^2)	9.6 ± 3.9	11.9 ± 7.2	3.7 ± 2.9*	8.5 ± 2.5	Genotype *P* = 0.0047; Treatment *P* = 0.0276; Interaction *P* = 0.4137
Smax (L/L_o)	0.37 ± 0.11	0.42 ± 0.07	0.33 ± 0.11	0.39 ± 0.02	Genotype *P* = 0.2412; Treatment *P* = 0.0998; Interaction *P* = 0.7863
Vmax (L_o/s)	4.5 ± 1.3	4.3 ± 1.7	3.1 ± 1.9	4.9 ± 0.9	Genotype *P* = 0.4947; Treatment *P* = 0.1557; Interaction *P* = 0.0564

David P. Burns is a PhD trainee at University College Cork, Ireland. His primary research interest is the control of breathing in muscular dystrophy, with wider interests in cardiorespiratory physiology in animal models of disease. He received the Usha Award of the American Physiological Society, which was presented at the Experimental Biology 2017 meeting in Chicago for research from his doctoral studies, published in The Journal of Physiology. David was selected as one of three early career scientists working in Ireland to participate at the 68th Nobel Lindau meeting in Germany. He will commence postdoctoral training in the United States later this year.